Northeastern University

Graduate School of Engineering

Dissertation Title: **Regular, Irregular, Functionally Graded, and Hierarchical Cellular Structures**

Author: **Amin Ajdari**

Department: **Department of Mechanical and Industrial Engineering**

Approved for Dissertation Requirement for the Doctor of Philosophy Degree

Professor Ashkan Vaziri Dissertation Advisor	Date
Professor Hamid Nayeb-Hashemi Dissertation Committee	Date
Professor George Adams Dissertation Committee	Date
Professor Hameed Metghalchi Department Chair	Date
Director of the Graduate School	Date

REGULAR, IRREGULAR, FUNCTIONALLY GRADED, AND HIERARCHICAL CELLULAR STRUCTURES

A DISSERTATION PRESENTED

BY

AMIN AJDARI

TO

THE DEPARTMENT OF MECHANICAL AND INDUSTRIAL ENGINEERING

IN PARTIAL FULFILLMENT OF THE REQUIREMENTS
FOR THE DEGREE OF

DOCTOR OF PHILOSOPHY

IN THE FIELD OF

MECHANICAL ENGINEERING

NORTHEASTERN UNIVERSITY
BOSTON, MASSACHUSETTS

DECEMBER 2011

ABSTRACT

From the structural point of view, cellular structures have properties that are much superior compared to the properties of the material that they are made of, including high strength to weight ratio and energy absorption. One of the key applications of the cellular structures is the design of structural components with superior energy absorption and impact resistance. Nowadays, the application of cellular structures has been extended in various fields of engineering. In this perspective, it is vital to develop a detailed understanding of the relationship between mechanical properties and microstructure of cellular materials.

We investigate the in-plane dynamic crushing of two-dimensional cellular structures using finite element methods. Both regular and randomly-distributed cellular structures, as well as functionally graded cellular structures are considered and their response is modeled up to large crushing strains. We have also studied the energy absorption of hierarchical honeycombs where every three-edge vertex of a regular hexagonal lattice is replaced with a smaller hexagon.

Our numerical simulations of in-plane dynamic crushing of cellular structures show three distinct deformation shapes of regular hexagonal cellular materials: quasi-static, moderate-rate dynamic mode and high-rate dynamic mode. Special attention was made towards quantifying the energy absorbent characteristics of the cellular structure as a function of cellular structure relative density and impact velocity, as well as the density gradient for functionally graded structures, where a relative density gradient in the direction of crushing was introduced in the computational models by a gradual change of the cell wall thickness. Decreasing the relative density in the direction of crushing was shown to enhance the energy absorption of honeycombs at early stages of crushing. Our results also showed that hierarchical honeycombs of first and

second order can be up to 2.0 and 3.5 times stiffer than regular honeycomb at the same mass (i.e., same overall average density) and they have advanced energy absorption capacity compared to regular honeycomb with the same mass. The results provide new insight into the behavior of engineered and biological cellular materials, and could be used in development of a new class of energy absorbent cellular structures.

ACKNOWLEDGEMENTS

I wish to express my deep gratitude to Professor Ashkan Vaziri, my academic advisor, for his guidance, constant encouragement, and his valuable advice in last four years. But more than that, it is his personal warmth that has made working with him such a valuable experience for me.

I would like to express my sincere appreciation to Professor Hamid Nayeb-Hashemi for his support both technically as well as emotionally, and for the valuable suggestions and stimulating discussions we have had. I would not have been able to complete this work without his help.

This acknowledgement would be incomplete, if I miss to mention the support I received from my research group, specially Babak Haghpanah Jahromi and Jim Papadopoulos for their fruitful discussions. I would also want to thank my family for their everlasting love and unconditional encouragement throughout my whole life. Without their help and support, I wouldn't be able to make this happen.

TABLE OF CONTENTS

LIST OF FIGURES

1 CHAPTER 1: INTRODUCTION

1.1 Cellular structures: Applications and background

Cellular structures extend the range of properties available to the engineers. Emergence of robust methods for fabrication of cellular structures, such as wire assembly and perforated sheet folding, have augmented their usage as lightweight and multifunctional materials. From the structural point of view, cellular structures have properties that are much superior compared to the properties of the material that they are made of, including high strength to weight ratio and energy absorption (Gibson, 1997). The application of cellular structure ranges from architectural masterpieces of Antonio Gaudi (Nonell, 2001) to thermal insulators (Lu and Chen, 1999) and three dimensional scaffolds for tissue engineering (Hollister, 2005; Hutmacher, 2000).

One of the key applications of the cellular structures is the design of structural components with superior energy absorption and impact resistance. The basic applications pertaining to these characteristics are packaging of fragile components (e.g. electronic devices) and various protective products like helmets and shielding. Another emerging application in this area is usage of cellular structures as the core material for metal sandwich panels, which are shown to have superior performance over the counterpart solid plates of equal mass under shock loading (Dharmasena et al., 2009; Liang et al., 2007; Mori et al., 2009; Mori et al., 2007; Rathbun et al., 2006; Vaziri and Hutchinson, 2007; Vaziri et al., 2007; Wadley et al., 2008; Wadley et al., 2007; Wei et al., 2008; Xue and Hutchinson, 2003, 2004; Xue and Hutchinson, 2006). Core topology and relative density have considerable influence on performance of the sandwich panels, as the core crushes at early stage of deformation and absorbs a large fraction of the kinetic energy imparted to the panel due to shock loading (Fleck and Deshpande, 2004; Hutchinson and Xue, 2005) – Thus, there is driving need to better understand the behavior of cellular structure under dynamic loading.

In the quasi-static regime, the crushing response of most metal cellular structures shows a typical stress–strain curve that includes three regimes: an elastic response followed by a plateau regime with almost constant stress and eventually a densification regime of sharply rising stress (Jang and Kyriakides, 2009a, b; Mohr et al., 2006; Papka and Kyriakides, 1998; Triantafyllidis and Schraad, 1998). Under dynamic crushing, however, the response of the metallic cellular structure is governed by complex localized phenomena that include buckling and micro-inertial resistance. The fundamental study of Vaughn et al. (2005) and (Vaughn and Hutchinson, 2005) has provided much insight into these effects, including the interaction between plastic waves and localized buckling under dynamic loading. (Xue and Hutchinson, 2006) showed that micro-inertial resistance of the core webs of a square honeycomb metal core increases its resisting force remarkably at early stages of dynamic crushing. At later stages of deformation, the dynamics effects results in suppression of the buckling of the metal webs, leading to emergence of buckling shapes with a wavelength much smaller than the core height. These effects lead to a remarkable increase in the plastic energy dissipation of honeycombs under dynamic crushing at high strain rates (Rathbun et al., 2006; Xue and Hutchinson, 2006). In a complementary study, (Vaziri and Xue, 2007) studied the role of strain rate on the crushing response of folded plate and truss cores. Their study showed that the initial elevation in the resisting stress of the metal cores due to the micro-inertial resistance mainly depends on the core relative density and strain rate and is relatively insensitive to the core topology.

1.2 Objectives

To further explore the effect of strain rate on the crushing behavior and energy absorption of cellular structures, we have studied the response of two dimensional regular hexagonal honeycomb under impact and in-plane dynamic crushing, Chapter 2. Most of the previous work performed on the mechanical behavior of cellular materials, including the results in Chapter 2, considers an intact structural organization for the cellular material. However, most engineered cellular materials do not have a perfect structural organization. In Chapter 3, we have investigated the role of defects, and more specifically missing cell clusters on the overall dynamic behavior of hexagonal honeycombs. The response of two dimensional Voronoi cellular structures with different level of irregularities is also discussed. Our study complements previous studies on the dynamic behavior of cellular structures with uniform cell size and wall thickness (Hönig and Stronge, 2002a, b; Li et al., 2007; Liu and Zhang, 2009; Ruan et al., 2003; Zhao and Gary, 1998; Zheng et al., 2005; Zou et al., 2009), while providing new insight into the role of deformation rate, defects and irregularity on the behavior of cellular structures under dynamic loading. In Chapter 4, we explore the behavior of functionally graded cellular structures and carry out a systematic study to investigate the role of relative density gradient on the overall crushing response of cellular materials. In Chapter 5, we investigated the mechanical behavior of two-dimensional hierarchical honeycomb structures using analytical, numerical and experimental methods. There, we have presented a systematic way to incorporate hierarchy in honeycomb structures. The resulting isotropic in-plane elastic properties (effective elastic modulus and Poisson's ratio) of this structure are controlled by the dimension ratios for different hierarchical orders. Chapter 6, draws the attention to the dynamic response and energy absorption of hierarchical honeycombs. Conclusions are drawn in Chapter 7.

2 CHAPTER 2: IMPACT AND DYNAMIC CRUSHING OF REGULAR HEXAGONAL HONEYCOMBS

2.1 Background

In this part of the study, we developed finite element models of honeycomb structures with regular hexagonal cell shape to study their structural response under impact and in-plane crushing. First, we developed an algorithm to generate the geometry of the cellular materials in Matlab® (Mathworks Inc., Natick, MA). The developed geometrical models were imported into ABAQUS (SIMULIA, Providence, RI). Dynamic explicit solver with general frictionless contact available in ABAQUS was used to simulate the dynamic response of the honeycombs under impact and crushing as discussed below. To use the general contact option available in ABAQUS, each developed geometrical model was extruded normal to its cross section to create three dimensional models of honeycombs. The model was meshed with 4-node shell elements and plain strain condition was imposed to the model by constraining the out of plane degrees of freedom along the edges of the cell walls. A mesh sensitivity analysis was carried out to ensure that the results are not sensitive to the mesh size. In all the calculations, we assumed the cell wall material to be linear elastic – perfectly plastic with Young's modulus, $E = 70\ GPa$, yield strength, $\sigma_Y = 130\ MPa$, Poisson's ratio, $v = 0.3$, and density, $\rho = 2700\ kg/m^3$, which are typical properties of aluminum. For a regular hexagonal honeycomb, the effective yield stress can be calculated from $\sigma_{Yc} = 0.5\,\rho_c^2\sigma_Y$, where ρ_c is the relative density of the honeycomb, defined as the area fraction of the cell walls with respect to the structure's dimensions (Gibson, 1997). In all the calculations presented in this study, the relative density of the honeycombs was varied by changing the thickness of the cell walls. We investigated several cases, where the relative density was changed by varying the cell wall size, while keeping the thickness constant. Our results showed that varying the cell wall size does not have significant effect on the crushing

response of regular hexagonal honeycombs, as long as the relative density of cellular structure is kept constant.

2.2 Impact behavior of honeycombs

To simulate the impact response of the hexagonal honeycomb, a rigid flat plate with mass, M was modeled to impact the honeycomb with an initial velocity, V_0, as shown schematically in Figure 2-1-A. The honeycomb was taken to be clamped at its bottom surface. Periodic boundary condition was applied in each side of the structure to avoid the influence of the model boundaries on the simulation results (Harders et al., 2005). After the impact, the rigid plate comes to rest as it crushes the honeycomb structure and finally detaches from it with a velocity that is much lower (generally less than 2% of the impact velocity) than its initial impact velocity. The initial kinetic energy of the rigid plate is $MV_0^2/2$, which is mainly absorbed by the plastic deformation of the cell walls as the honeycomb is crushed by the rigid plate. Figure 2-1-B shows the crushing response of honeycombs with three different relative densities, quantified as the average crushing of the cellular material, $\varepsilon = \delta/L$, where δ is the crushing displacement and L is the honeycomb height in the crushing direction, versus the actual time, t, normalized by $t_0 = L/V_0$. The results shown in Figure 2-1-B represent a constant normalized initial kinetic energy of the rigid plate, $\overline{KE} = (MV_0^2/2)/(\sigma_{Yc}AL)$, where σ_{Yc} is the theoretical effective yield stress of the honeycomb, A is the cross-section area of the structure normal to the longitudinal direction. $\sigma_{Yc}AL$ is a theoretical estimate of the energy dissipated by plastic deformation in a bar made of a perfectly plastic material with yield stress, σ_{Yc}, height L and section A, when it get crushed to 100% strain. Under rigid plate impact, the maximum crushing of honeycomb, ε_{max}, and the corresponding crushing time (i.e. at which the rigid plate has zero velocity), t_s, depends on the relative density of the structure and the impact velocity, as quantified in Figure 2-1-C and

Figure 2-1-D for a wide range of normalized initial kinetic energies of the rigid plate and honeycomb relative densities. In this set of calculations, the initial kinetic energy of the rigid plate was varied by changing the plate initial velocity, while its mass were kept constant. Based on the assumption that the total initial kinetic energy of the rigid plate is dissipated by the plastic deformation of the honeycomb, the maximum crushing of the honeycomb can be estimated from, $MV_0^2/2 = \sigma_{Yc} AL\varepsilon_{max}$. This yields $\varepsilon_{max} = \overline{KE}$, which is plotted in Figure 2-1-C as a solid line, along with the results from detailed finite element calculations.

Similarly, an estimate for the t_s can be obtained using the principal of impulse and momentum, $\sigma_{Yc} A t_s = MV_0$, where $\sigma_{Yc} A$ is the force applied by a structure made of a perfectly plastic material with yield strength of σ_{Yc}. Dividing both sides of this equation by t_0, gives: $t_s/t_0 = MV_0^2/\sigma_{Yc} AL = 2\overline{KE}$, which is shown in Figure 2-1-D. For low values of normalized kinetic energy, where the crushing strain is not high, the numerical results are in good agreement with the theoretical estimate. However, for high values of initial kinetic energy, the numerical simulations predict $\varepsilon_{max} < \overline{KE}$ due to the dynamic effects and nonlinearity caused by cell walls contact. For a perfectly plastic material, the role of the micro-inertial resistance of core walls is minimal and thus, the effective yield strength of honeycomb is approximately equal to the honeycomb yield strength (Xue and Hutchinson, 2006). However, at high strain rate, the contact between the cell walls increases the effective yield strength of the honeycomb, leading to elevation of the effective yield strength of honeycombs.

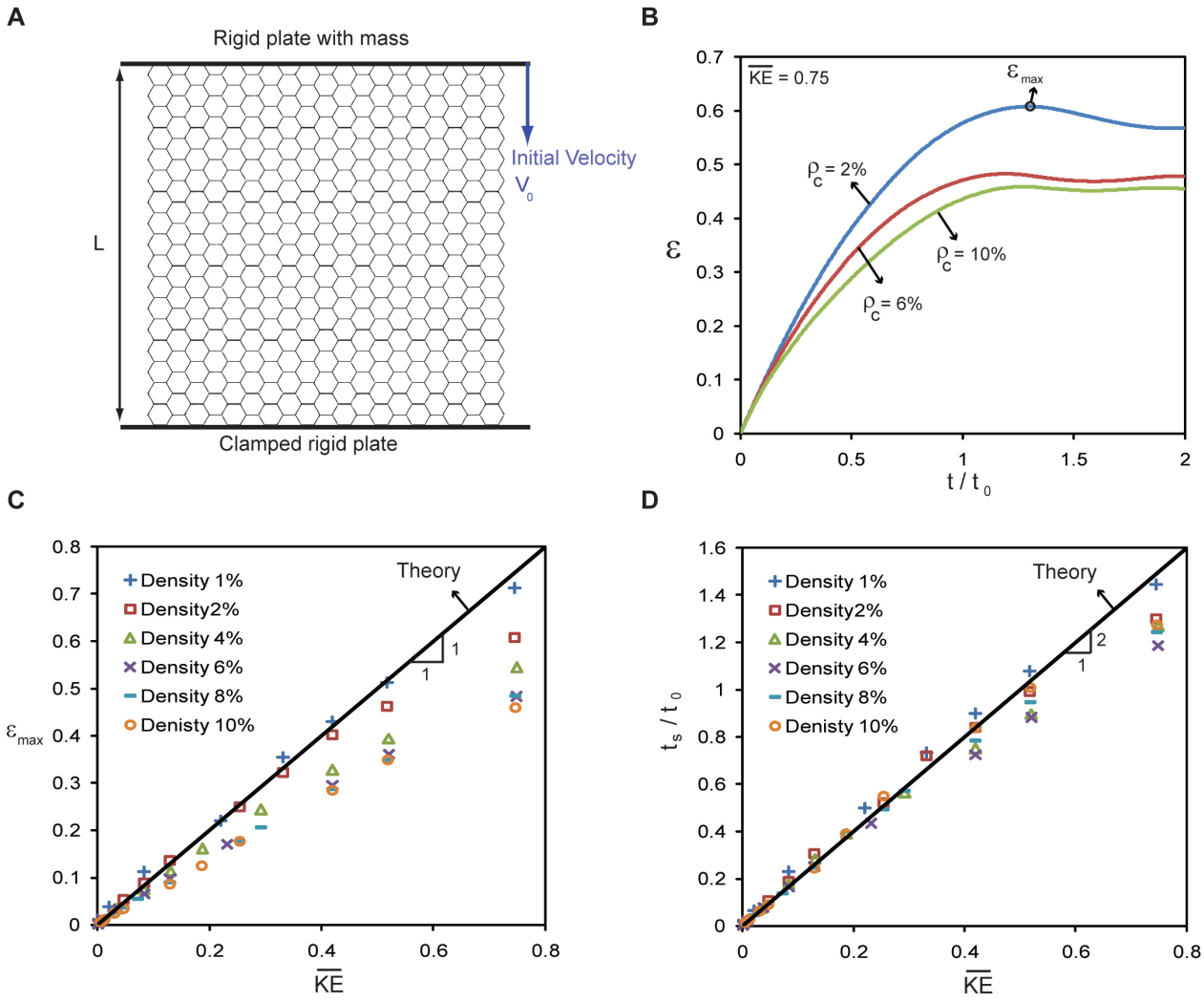

Figure 2-1- Impact response of a regular hexagonal honeycomb. (A) Schematic of the finite element model. (B) The crushing response of honeycombs with three different relative densities. (C) The maximum crushing strain of honeycomb versus the normalized initial kinetic energy of the rigid plate. (D) The normalized crushing time versus the normalized initial kinetic energy of rigid plate. The solid lines show the theoretical estimates. The markers show the finite element results.

2.3 Dynamic crushing of honeycombs

To explore the energy absorption of honeycombs under dynamic crushing, we have also simulated the honeycomb response under in-plane dynamic crushing at a constant prescribed velocity, V, as shown schematically in Figure 2-2-A. Similar to the previous simulations, the honeycomb was clamped along its bottom edge and periodic boundary conditions were imposed at its sides. An important dimensionless parameter which governs the inertial effects is $\bar{V} = V/(c_0\varepsilon_Y)$, where $c_0 = (E/\rho)^{0.5}$ is the elastic wave speed in the cell wall material, and $\varepsilon_Y = \sigma_Y/E$ (Xue and Hutchinson, 2006).

Figure 2-2-B shows the normalized plastic energy dissipation, $\bar{U}_P = U_P/\sigma_{Yc}AL$ of honeycomb, where U_P is the plastic energy dissipation calculated directly from the numerical simulations for two different crushing velocities, $\bar{V} = 0.32$ and $\bar{V} = 6.35$. At low crushing rates, the normalized dissipated plastic energy increases slightly by increasing the structure relative density. However, all honeycombs have comparable normalized plastic energy absorption.

In contrast at high crushing velocities, the normalized plastic energy dissipation of a honeycomb strongly depends on its relative density and is higher for a honeycomb with lower relative density, which is due to dynamic effects and the nonlinearity caused by cell walls contact as discussed for honeycombs subjected to impact rigid plate. In Figure 2-2-C, we have quantified the normalized plastic energy dissipation of regular honeycombs with $0.01 \leq \rho_c \leq 0.10$, under dynamic crushing. The results are presented in the log-log scale and at $\varepsilon = 0.5$ or 50% crushing.

At low crushing rates, $\bar{V} < 1$, the normalized plastic energy dissipation of the honeycomb increased by increasing its relative density. For $\bar{V} > 1$, honeycombs with smaller relative density have remarkably higher normalized plastic energy dissipation at the same level of crushing strain. Moreover, we have studied the deformation modes of the honeycomb under dynamic crushing. Three distinct deformation shapes, which depend on the crushing rate and honeycomb relative density, are identified for the regular honeycombs as shown in Figure 2-3-A: quasi-static or X-shape, transition or V-shape, and dynamic shape.

In Figure 2-3-B, we provided a deformation map for regular honeycomb structures subjected to dynamic crushing. The critical normalized crushing rate associated with the transition between different modes, $\bar{V}_c$ increases approximately linearly with increasing the relative density, as shown in Figure 2-3-B by the dotted lines.

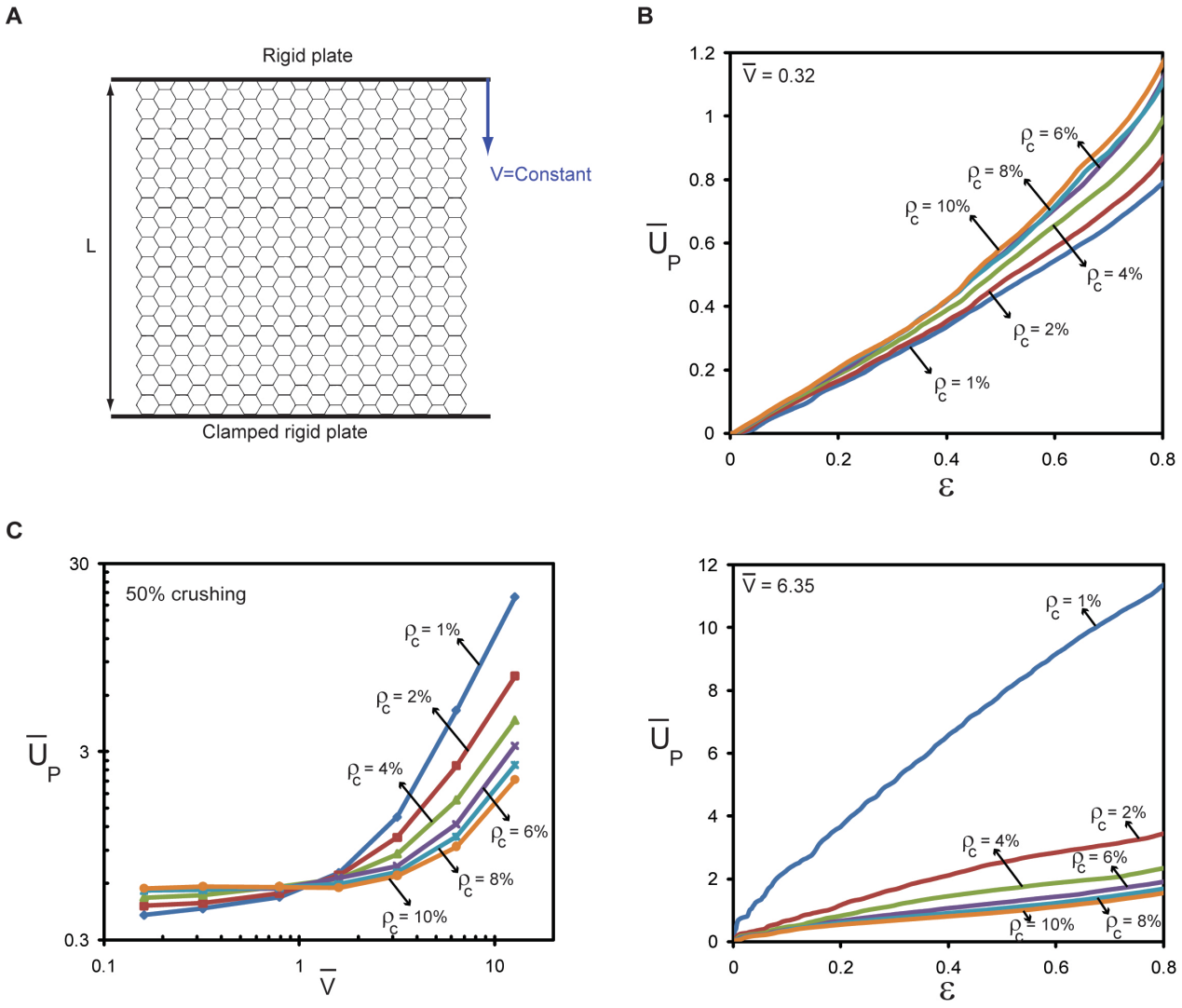

Figure 2-2- Dynamic crushing of a hexagonal regular honeycomb. (A) Schematic of the finite element model. (B) Normalized plastic energy dissipation versus the crushing strain for $\bar{V} = 0.32$ and $\bar{V} = 6.35$. (C) The normalized plastic energy dissipation of regular honeycombs versus the normalized crushing velocity at 50% crushing. The results in (C) are presented in the log-log scale.

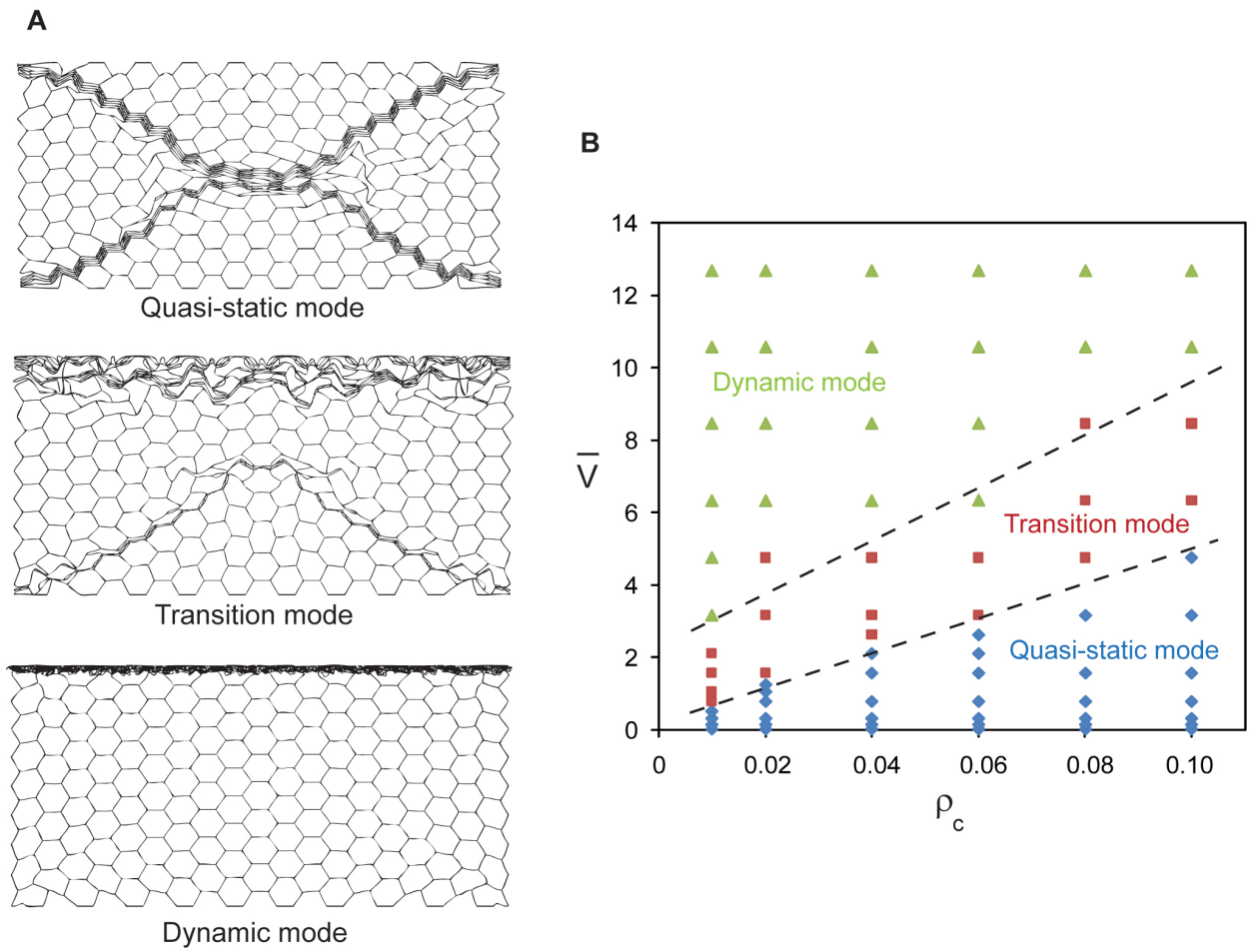

Figure 2-3- Deformation modes of a hexagonal regular honeycomb. (A) Three distinct deformation shapes. (B) Deformation map for a regular honeycomb subjected to dynamic crushing. The markers show the finite element results. The dotted lines show the approximate limit associated with the transition between different deformation modes.

3 CHAPTER 3: DYNAMIC CRUSHING OF IRREGULAR CELLULAR STRUCTURES

3.1 Background

In contrast to an idealized structure studied in Chapter 2, most cellular materials have inherent imperfections and in-homogeneities in their structural organization. Typical types of imperfections are missing walls and variations in the arrangement of cell walls, cell size and wall thickness. These structural variations are ubiquitous in natural cellular materials (e.g. cork, sponge and toucan beak) and cellular structures manufactured using random physical processes (e.g. foams). They also could appear in engineered cellular structures that are designed to have uniform cellular arrangement, due to fabrication errors.

Several studies have been carried out to investigate the effect of different defects and structural variations on the quasi-static behavior of cellular structures (Ajdari et al., 2008; Chen et al., 1999; Fazekas et al., 2002; Fortes and Ashby, 1999; Guo and Gibson, 1999; Silva and Gibson, 1997; Silva et al., 1995; Wang and McDowell, 2003; Zhu et al., 2001a). (Liu and Zhang, 2009) studied the dynamic crushing behavior of honeycombs with different cell topologies and arrangements. Their results suggest that the energy absorption of a honeycomb depends not only on the structure relative density, but also on the cellular arrangement and irregularity. In the same context, (Zheng et al., 2005) showed that cell arrangement irregularity elevates the energy absorption of two- dimensional cellular structures. Somewhat contradictory results were reported by (Tan et al., 2005), who suggested that the irregularity in the cell arrangement does not have considerable effect on the plastic energy absorption of a cellular structure.

In this chapter, we have studied the role of irregularities in the structural organization of cellular structure subjected to in-plane dynamic crushing. Specifically, we considered two types of irregularities: In section 3.2, we investigated the role of a missing wall cluster on the energy

absorption of a regular hexagonal honeycomb. In section 3.3, we discussed the dynamic crushing of irregular cellular structures.

3.2 Regular hexagonal honeycombs with missing wall clusters

Schematics of honeycombs with a missing cell cluster of two different sizes, corresponding to 5% and 10% missing walls (defect), are shown in Figure 3-1-A. In this figure, the missing cell cluster is located at the center (mid height) of the cellular structure. The defect size is quantified as the number of missing walls to the total number of cell walls. For example, a missing wall cluster denoted by '5% defect', indicates that the 5% of adjacent cell walls were removed from the model to form the missing wall cluster - Thus, the average relative density of the cellular structure was decreased by 5%. Similar boundary conditions as those used in chapter 2 were imposed for this investigation. To study the effect of missing cluster on the overall energy absorption of honeycombs, we considered honeycombs with two different relative densities, $\rho_c = 0.02$ and $\rho_c = 0.06$ subjected to a wide range of crushing velocities. In Figure 3-1-B, we plotted the normalized plastic energy dissipation of honeycombs with no defect and with two different missing wall cluster sizes at the crushing strain $\varepsilon = 20\%$ for a wide range of crushing velocities. The overall plastic energy absorption of a honeycomb does not change significantly with the presence of a missing wall cluster as large as 5%. However, the honeycomb with 10% defect has considerably lower plastic energy dissipation compared to the regular honeycomb with no defect at both low and high crushing velocities. The normalized plastic energy dissipation of the honeycombs with $\rho_c = 0.02$ and $\rho_c = 0.06$ at the 50% crushing is quantified in Figure 3-1-C. Again, the honeycomb with 10% defect shows a considerably lower energy absorption compared to the honeycomb with no defect.

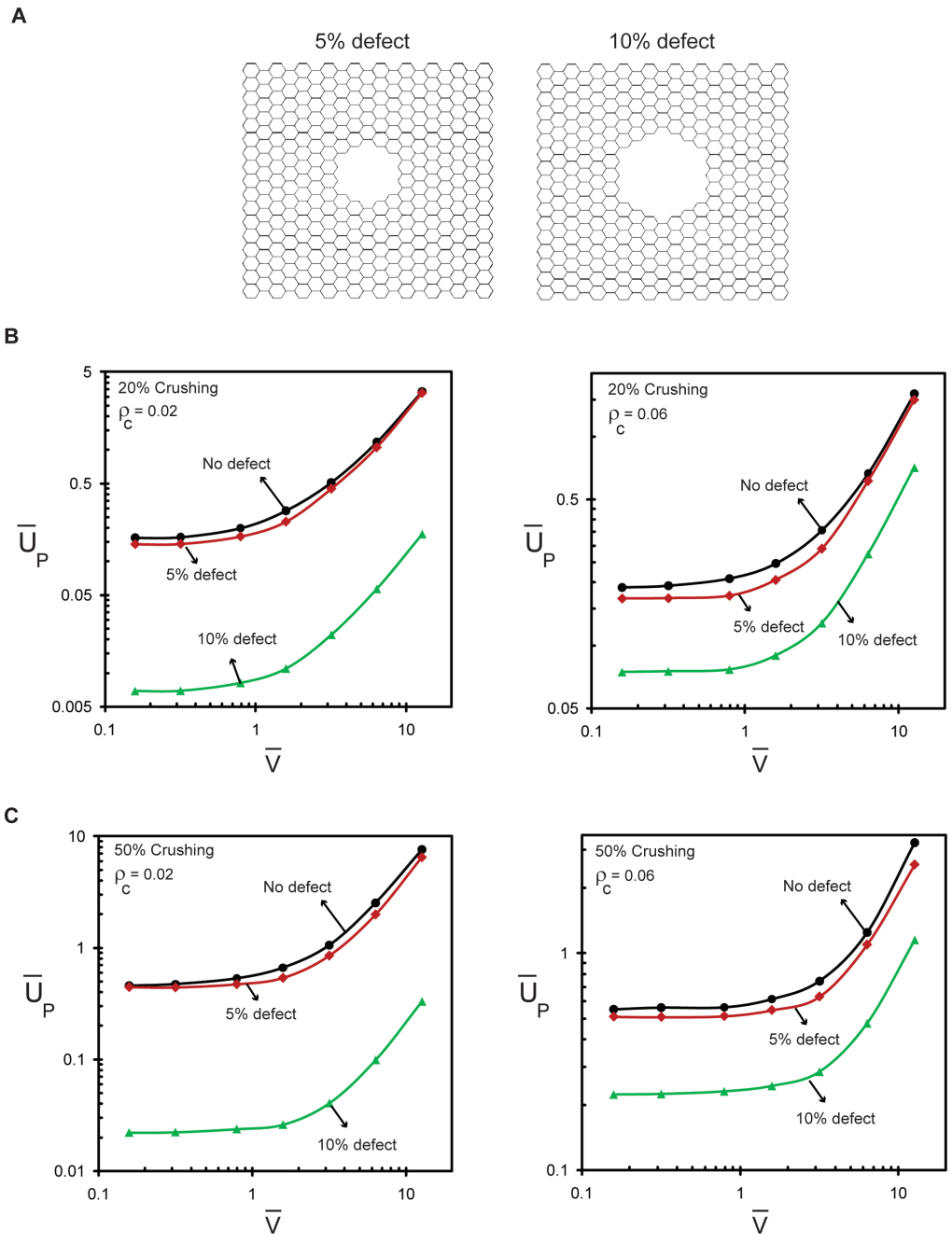

Figure 3-1- Role of missing cell cluster size. (A) Schematic of honeycombs with a missing cell cluster of two different sizes. (B) and (C) The normalized plastic energy dissipation of honeycombs with $\rho_c = 0.02$ and $\rho_c = 0.06$ versus the normalized crushing velocity at 20% and 50% crushing, respectively. The results for honeycombs with no defect and with 5% and 10% defects.

In Figure 3-2, we have plotted the normalized plastic energy of honeycombs with $\rho_c = 0.02$ and $\rho_c = 0.06$ and a missing wall cluster of different sizes divided by the normalized plastic energy of the counterpart honeycomb with no defect, as a function of normalized crushing velocity. The results are presented for honeycombs with 5% and 10% defects at 20% and 50% crushing strains in Figure 3-2-A and Figure 3-2-B, respectively. These plots quantify the role of the missing wall cluster on the energy absorption of cellular structure. The amount of reduction in the plastic energy absorption of the honeycomb due to the presence of the defect is not considerably sensitive to the crushing velocity. Our results suggest that the energy absorption capacity of honeycombs with a lower relative densities, are more sensitive to the presence of a defect. For example, for a honeycomb with $\rho_c = 0.02$ and 10% missing cluster, the normalized plastic dissipation decreases about 95% compare to that of regular honeycomb with no defect. In contrast, for a honeycomb with $\rho_c = 0.06$, and 10% missing cluster, the reduction is about 60%, as shown in Figure 3-2.

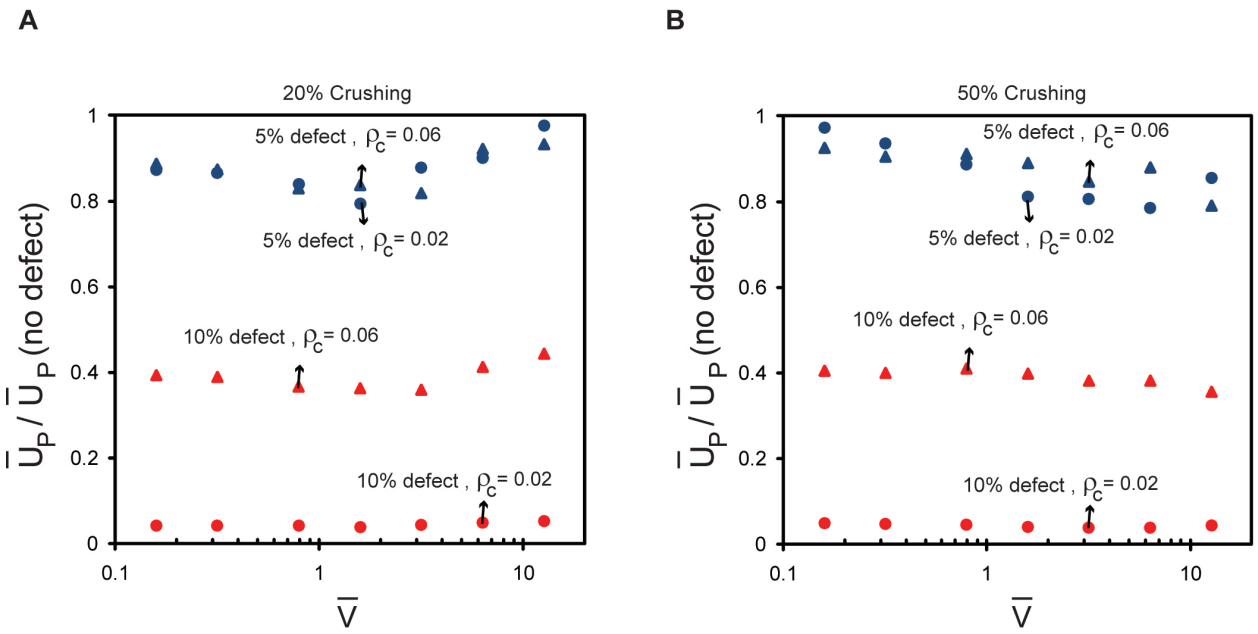

Figure 3-2- (A) The plastic energy dissipation of honeycombs with 5% and 10% defects normalized by the plastic energy dissipation of a honeycomb with no defect versus the normalized crushing velocity at 20% and 50% crushing, respectively. The results are presented for honeycombs with $\rho_c = 0.02$ and $\rho_c = 0.06$.

In Figure 3-3, we have studied the role of cluster location on the plastic energy absorption of a honeycomb under dynamic crushing. In this set of calculations, three models of honeycombs with 5% defect were analyzed with a missing cluster located at three different locations along the height of the cellular structure: 1) the missing wall cluster considered close to the rigid plate; 2) the missing wall cluster is at the mid height (as shown in Figure 3-3-A) ; and 3) the missing wall cluster close to the clamped side. Figure 3-3-B shows the results of the simulations presented in the form of normalized plastic energy dissipation versus the crushing strain for honeycomb with $\rho_c = 0.06$ and subjected to $\bar{V} = 6.35$. At this crushing rate, the deformation of honeycomb under crushing is limited to the crushing side (dynamic mode, Figure 2-3). Thus, a missing cluster closer to the rigid plate affects the energy absorption of the honeycomb at early stages of crushing. For example, a honeycomb with a missing cluster in location 1 (Figure 3-3) shows smaller plastic energy dissipation compared to a honeycomb with no defect at crushing strain of $\varepsilon < 0.1$ (i.e. at early stage of deformation). However, the plastic energy dissipation only gets altered at crushing strain $\varepsilon > 0.4$ for honeycomb with 5% defect located close to its clamped side (location 3). We also checked that changing the location of the missing cell cluster in the direction normal to the crushing direction does not have a considerable effect on the plastic energy absorption of honeycombs. The results are not presented for brevity.

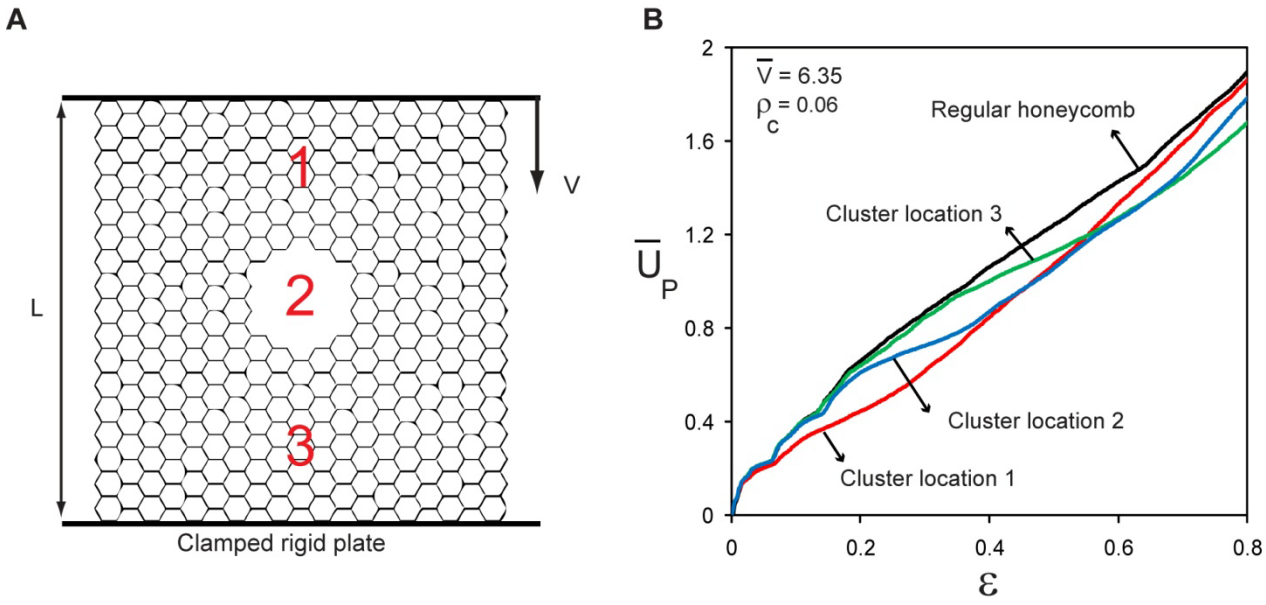

Figure 3-3- Role of missing cell cluster location. (A) Different models of honeycombs with 5% defect located at three different locations along the height of the structure (1,2 and 3). (B) Normalized plastic energy dissipation versus the crushing strain for honeycomb with $\rho_c = 0.06$ and subjected to dynamic crushing with $\bar{V} = 6.35$.

3.3 Irregular cellular structures

In this section, we studied the role of irregularity in the form of variation in arrangement of cell walls on the dynamic behavior and energy absorption of cellular structures under crushing. Specifically, we studied the dynamic crushing of irregular structures. To construct the models of cellular structures, we started from a set of points located at the centroids of a regular hexagonal honeycomb, where each point is located at distance $\sqrt{3}l$ from its adjacent points – see Figure 3-4-A.

To introduce irregularity in the cell arrangement, each point was moved randomly in both in-plane coordinates by $\alpha_i = \emptyset_{i1} \times D/l$ and $\beta_i = \emptyset_{i2} \times D/l$, where subscript i denotes the point number, D is the the maximum dislocation of the initial points and is defined here as 'irregularity index' and $0 \leq \emptyset_{i1}, \emptyset_{i2} \leq 1$ are random numbers generated for each point separately. Then, the Voronoi diagram which is generated by constructing the perpendicular bisectors of each pair of adjacent points (Silva et al., 1995; Zhu et al., 2001b), was used to generate the models of the irregular cellular structures. Application of the Voronoi diagram to the original reference points (i.e. $D/l = 0$) gives the arrangement of a regular hexagonal honeycomb. Examples of structures with $D/l = 1$ and $D/l = 2$ are shown in Figure 3-4-B. It should be noted the arrangement of a cellular structure with a given cell size and irregularity index changes each time the model is constructed, since $\emptyset_{i1}$ and $\emptyset_{i2}$ are generated in each trial separately.

Figure 3-4-C shows the normalized plastic energy dissipation versus the crushing strain for three irregular cellular structures with $D/l = 1, 2$ and 3 and relative density $\rho_c = 0.06$. The plot shown for each irregularity index is the average results obtained for six different irregular

structure models. The standard deviations from the results at several different crushing strains are also shown.

The result for a regular honeycomb is also presented for comparison. These results show that the irregularity does not have a considerable effect on the normalized energy dissipation of the cellular structures studied.

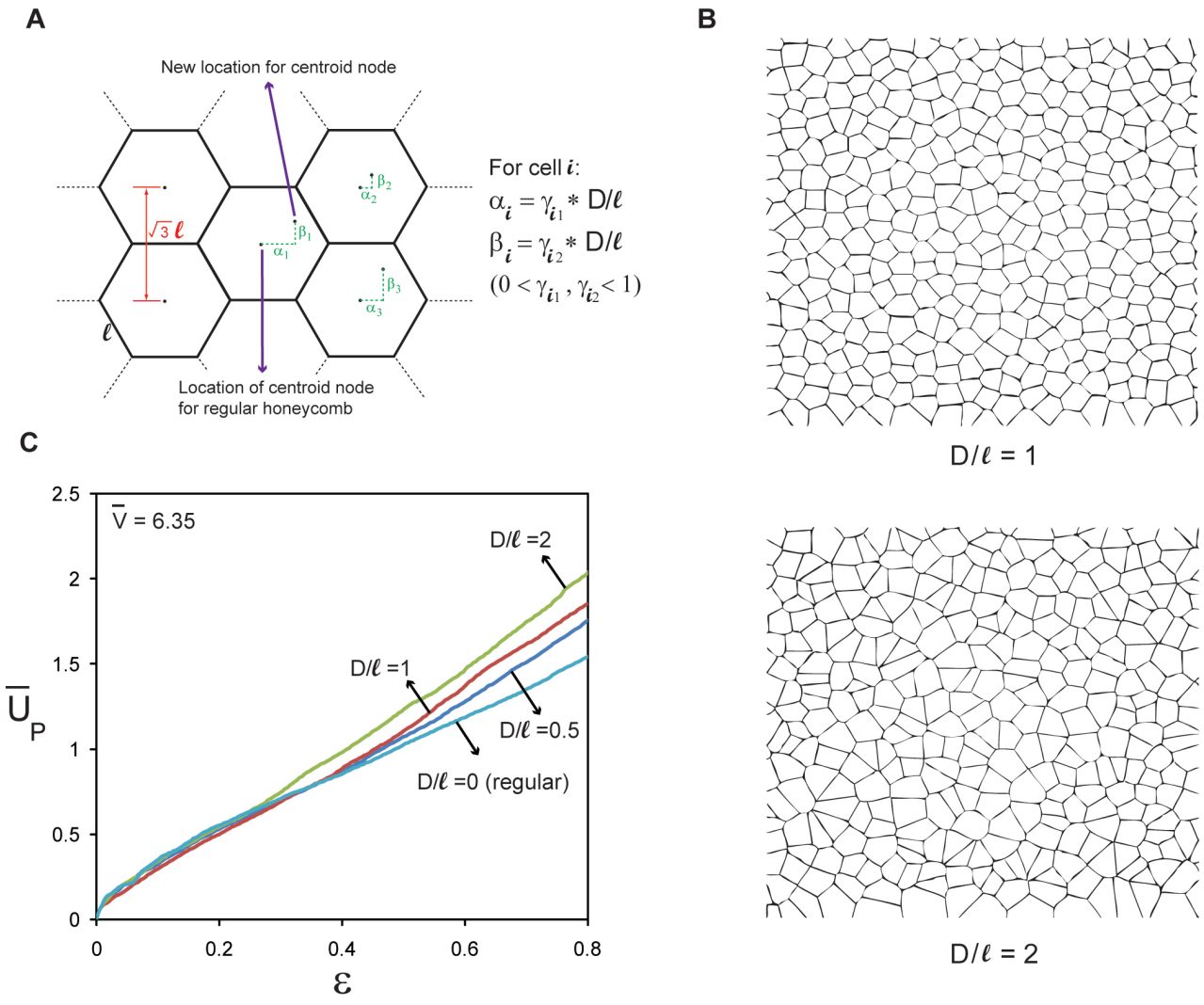

Figure 3-4- Dynamic crushing of irregular honyecombs. (A) Schematic of a regular hexagonal structures and location of centroids for irregular structures. (B) Irregular honyecombs with $D/l = 1$ and $D/l = 2$. (C) Normalized plastic dissipation of irregular structures with different irregularity indexes versus the crushing strain at $\bar{V} = 6.35$.

4 CHAPTER 4: DYNAMIC CRUSHING OF FUNCTIONALLY GRADED CELLULAR STRUCTURES

4.1 Background

Functionally graded materials (FGM) consist of a gradual change in the volume fraction or mechanical properties of constituents in a direction. Application of these materials tends to reduce stresses resulting from material property mismatch, increases the bonding strength, improves the surface properties and provides protection against adverse thermal and chemical environment. Functionally graded materials are ideal for applications involving severe thermal gradients, ranging from thermal structures in advanced aircraft and aerospace engines to computer circuit boards (Abd El-Sayed et al., 1979; Evans et al., 1998; Gent, 1963; Gent and Thomas, 1959; Gibson, 1997; Ko, 1965; Lederman, 1971; Menges and Knipschild, 1975).

Cellular structures are a class of materials with low densities and novel physical, mechanical, thermal, electrical and acoustic properties. A gradual increase in the cell size distribution, can impart many properties such as mechanical shock resistance and thermal insulation. The understanding of mechanical properties of functionally graded cellular structures as a function of cell size gradient is important in the proper application and utilization of these materials. Furthermore, the presence of defects may affect the material properties of graded cellular structures.

Several efforts have been made to investigate the mechanical behavior and the effects of imperfections on the mechanical properties of cellular materials; most of which are based on the finite element method (FEM) . (Chen et al., 1999) investigated the influence of different types of morphological imperfections (waviness, non-uniform cell wall thickness, cell-size variations, fractured cell walls, cell-wall misalignment and missing cells) on the yielding of 2D cellular solids. They also performed a finite element study to determine the effects of holes on elastic modulus and yield strength of regular honeycombs under biaxial loading. (Wang and McDowell,

2003) and (Silva and Gibson, 1997) investigated the effects of missing or fractured cell walls on mechanical properties of regular hexagonal and Voronoi cellular materials. In mu previous work, (Ajdari et al., 2008) we investigated the compressive uniaxial and biaxial behavior of functionally graded Voronoi structures, using finite element methods Furthermore, the effect of missing cell walls on its overall mechanical (elastic, plastic, and creep) properties is investigated. The finite element analysis showed that the overall effective elastic modulus and yield strength of structures increased by increasing the density gradient. However, the overall elastic modulus of functionally graded structures was more sensitive to density gradient than the overall yield strength. The study also showed that the functionally graded structures with different density gradient had similar sensitivity to random missing cell walls. Creep analysis suggested that the structures with higher density gradient had lower steady-state creep rate compared to that of structures with lower density gradient. Here, we study the dynamic behavior of functionally graded cellular structures where a density gradient is introduced in the direction of crushing by changing the thickness of cell walls.

4.2 Energy absorption of functionally graded cellular structures

Functionally graded cellular structures are novel class of materials, where variations in cell size, shape and wall thickness results in a functional variation in the relative density and organization of the cellular structure. Examples of functionally graded cellular structures in nature are bamboo, banana peel and elk antler (Chen et al., 2008; Silva et al., 2006). Previous studies on impact resistance and energy absorption of functionally graded cellular structures have shown their potential for creating impact resistant structures and cushioning materials (Ali et al., 2008; Kiernan et al., 2009). (Cui et al., 2009) suggested that a functionally graded foam can exhibit superior energy absorption compared to a uniform foam with equal mass. In another

effort, (Wadley et al., 2008), constructed a multilayered pyramidal lattice from stainless steel and investigated the quasi-static and dynamic compressive response of these structures. The developed method allows fabrication of functionally graded cellular structures by varying the relative density of the pyramidal lattice at each layer.

In this study, we constructed finite element models of functionally graded cellular structures by changing the thickness of the cell walls - and thus, the relative density - in the direction of crushing. We divided a cellular structure to five equal-size regions with height $\Delta L = L/5$, and assigned different cell wall thicknesses to each region to introduce a constant density gradient, γ, in the cellular structure. The models were created for cellular structures with both regular hexagonal and irregular cellular arrangements – See Figure 4-1 and Figure 4-3, respectively. The density gradient, γ, was defined as $\gamma = (\rho_{i+1} - \rho_i)/\Delta L$, where ρ_i indicates the relative density of *i*-th region, as shown in Figure 4-1-A. γ = 0 gives a honeycomb with constant relative density, and a positive density gradient gives a cellular structure with a relative density that gradually decreases in the crushing direction. The total relative density of the structures was kept constant (here, $\rho_c = 0.05$), as the density gradient is introduced. For example, γ = 0.33 gives a cellular structure with a relative density that functionally decreases from 9% to 1% in the direction of crushing. However, the average density of this honeycomb structure is $\rho_c = 0.05$.

Figure 4-1-B and Figure 4-1-C show the energy absorption of functionally graded regular hexagonal honeycombs with different density gradients subjected to low velocity and high velocity dynamic crushing. As discussed above, the comparison between cellular structures with different density gradients are made at a constant average relative density. At both low and

high crushing velocities, the normalized energy absorption of honeycomb with a constant relative density, $\gamma = 0$, changes approximately linearly with the crushing strain.

At low crushing velocity ((i.e. quasi-static mode), introducing the density gradient decreases the energy absorption of the honeycombs up to crushing strains ~ 67%, and the honeycomb with $\gamma = 0$, has the maximum energy absorption for this crushing strain range. There are minimal differences between the response of functionally graded honeycombs with positive and negative density gradients, as quantified in Figure 4-1-B and expected in the quasi-static regime.

In contrast at high velocity crushing, the density gradient has a remarkable influence on the energy absorption of the honeycomb (Figure 4-1-C). Up to ~ 50% crushing, the functionally graded cellular structures with positive density gradient, $\gamma > 0$ - where the cellular structure relative density is high at the crushing side and changes gradually to its lowest value at the clamped side - have higher energy absorption compared to a honeycomb with $\gamma = 0$. The negative density gradient, $\gamma < 0$ results in reduction of the honeycomb energy absorption The influence of the density gradient on the energy absorption is very significant in early stages of crushing (i.e. crushing strain of up to 25%). At crushing strain ~ 56%, all honeycombs show similar energy absorption capacity ($\overline{U}_P \cong 1.5$ for all honeycombs). At higher crushing strains, honeycombs with a negative density gradient show considerable increase in their energy absorption capacity.

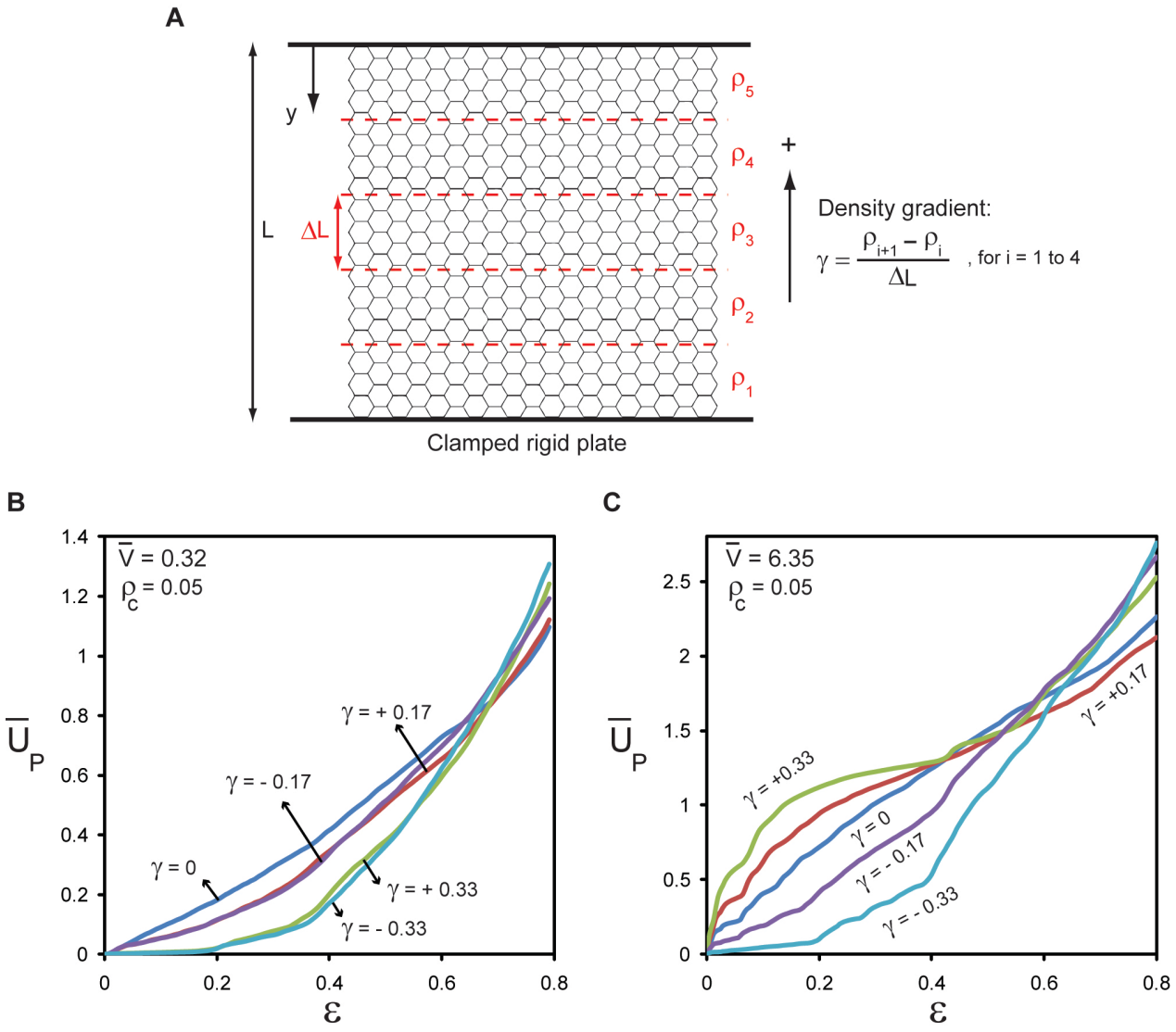

Figure 4-1- Dynamic crushing of a functionally graded regular hexagonal honeycomb. (A) Schematic of the model. (B) Normalized plastic energy dissipation versus the crushing strain for honeycombs with different density gradients at low crushing rates, $\bar{V} = 0.32$ and (C) at high crushing rate, $\bar{V} = 6.35$. The overall relative density of the honeycombs were kept constant, $\rho_c = 0.05$.

To explain these observations, we studied the deformation modes and the distribution of equivalent plastic strain of functionally graded honeycombs with $\rho_c = 0.05$ under crushing. Figure 4-2-A compared the deformation modes of a functionally graded honeycomb with $\gamma = 0.33$ and a honeycomb with a constant relative density, $\gamma = 0$ at 50% crushing. In the quasi-static regime ($\bar{V} = 0.32$), the deformation of the honeycomb with constant relative density is mainly concentrated along two bands, forming the X-Shape as explained in chapter 2. In Contrast, for a functionally graded honeycomb, the deformation is limited to the part of the structure with low relative density (close to the bottom in Figure 4-2-A), while the rest of the structure stays almost undeformed. At high velocity crushing ($\bar{V} = 6.35$), the deformation mode is quite different - see Figure 4-2-A: For a regular honeycomb with $\gamma = 0$, the deformation is highly localized to the crushing side – as described in details in chapter 2 – thus, only the cells close to crushing side undergo considerable deformation and contribute to the energy absorption of the honeycomb as it gets crushed. For cellular structures with $\gamma < 0$, the deformation mode is similar to that of regular honeycomb with $\gamma = 0$, and since the structure has a lower relative density at the crushing side, its overall energy absorption is even lower than its counterpart honeycomb with $\gamma = 0$. For a functionally graded honeycomb with $\gamma > 0$, the deformation is focused at both crushing and clamped sides of the honeycomb and thus, a higher number of cells deform and contribute to the overall energy absorption of the cellular structure, as can be seen in the deformed configurations shown in Figure 4-2-A.

To further understand the deformation modes of honeycombs, we have plotted the distribution of the equivalent plastic strain along the height of honeycombs with different density gradients in Figure 4-2-B and Figure 4-2-C. To calculate the equivalent plastic strain through the height of the structure, we averaged the equivalent plastic strains for all elements in each row

of the honeycomb from top to bottom. These plots shows the relative contribution of cells located at different heights of the structure on the overall energy absorption of the honeycomb. For the honeycomb with $\gamma = 0$ and subjected to $\bar{V} = 0.32$, all cell wall rows contribute to the overall energy absorption of the structure, by forming the X-shape deformation mode shown in Figure 4-2-A. At this crushing rate, for honeycombs with $\gamma > 0$, the cell walls with the lower relative density (wall thickness) are located near the clamped side and are mostly deformed under crushing, while for honeycombs with $\gamma > 0$, cell walls with lower density are located near the crushing side and gets more deformed compared to other cell walls. Figure 4-2-C shows the results for honeycombs with different density gradients at high crushing rates, $\bar{V} = 6.35$ at 50% crushing strain. For honeycombs with $\gamma \geq 0$, the cell walls near the crushing side are mainly deformed, while the induced plastic strains in cells located in the bottom half of the structure ($0.5 < y/L \leq 1$) is negligible. For honeycombs with $\gamma > 0$, cells at both side of the structure (crushing side and clamped side) gets strongly deformed under crushing, while the cells in the mid height of the structure contribute minimally to the overall energy dissipation of the cellular structure. It should be noted that the plastic energy dissipation of all honeycombs is comparable at this crushing strain, as can be seen in Figure 4-2-C and discussed above.

In Figure 4-3, we have repeated the calculations for an irregular cellular structure. The role of density gradient is more remarkable in this case compared to the regular hexagonal honeycombs, Figure 4-3-B. The deformation modes of irregular cellular structures with two different density gradients are displayed in Figure 4-3-C, which show qualitative agreement with the deformation mode of their regular hexagonal counterpart. Again, a higher number of cells of the structure with $\gamma = 0.33$, have deformed considerably, compared to the deformation mode of the counterpart irregular structure with $\gamma = 0$, which is highly localized at the crushing side.

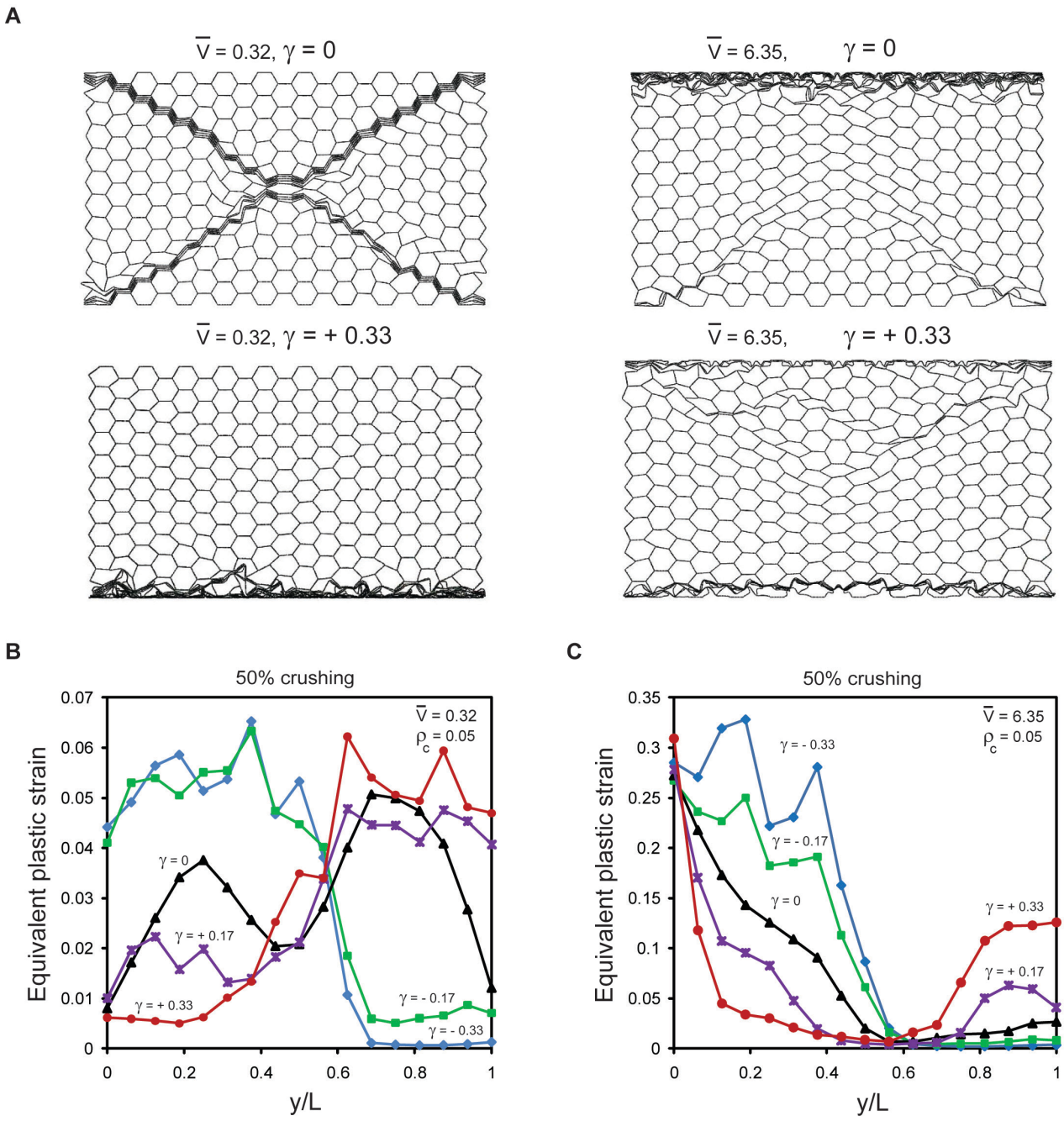

Figure 4-2- (A) Deformation shapes of regular cellular structures with constant and functionally graded relative density at 50% crushing at low and high crushing rates. (B) and (C) Equivalent plastic strain thorough the height of honeycombs with different density gradients subjected to $\overline{V} = 0.32$ and $\overline{V} = 6.35$, respectively, at 50% crushing. (The overall relative density of the honeycombs were kept constant, $\rho_c = 0.05$.

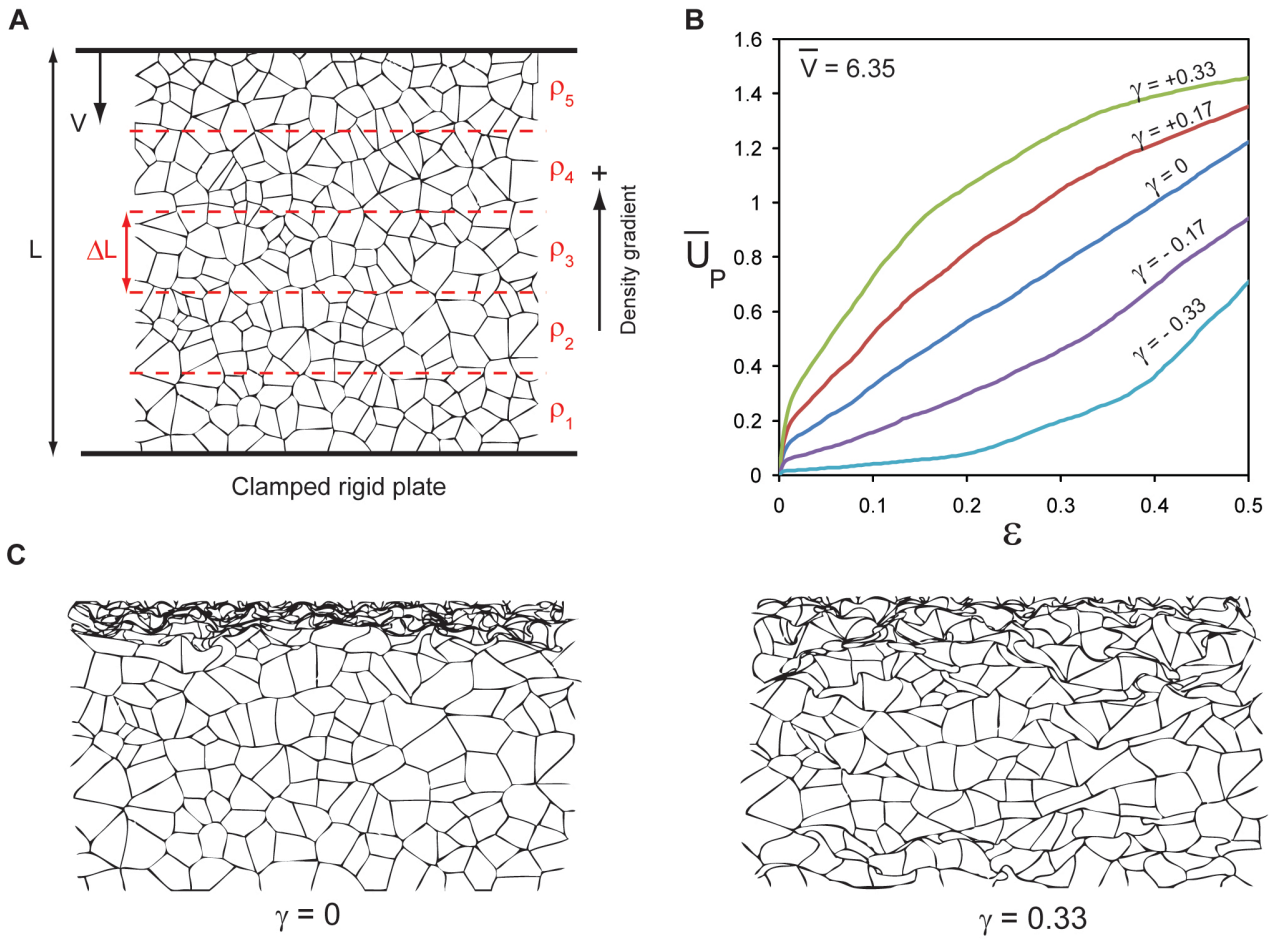

Figure 4-3- Dynamic crushing of a functionally graded irregular structure. (A) Schematic of the model of a functionally graded irregular cellular structure with $D/l = 2$. (B) Normalized plastic energy dissipation versus the crushing strain for an irregular cellular structures with different density gradients at the high velocity crushing, $\bar{V} = 6.35$. (C) The deformation shapes of irregular cellular structures.

5 CHAPTER 5: HIERARCHICAL HONEYCOMBS WITH TAILORABLE PROPERTIES

5.1 Introduction

Hierarchical structures are ubiquitous in nature and can be observed at many different scales in organic materials and biological systems (Aizenberg et al., 2005; Buehler, 2006; Espinosa et al., 2011; Fratzl and Weinkamer, 2007; Gibson et al., 2010; Lakes, 1993; Ortiz and Boyce, 2008; Qing and Mishnaevsky Jr, 2009). The hierarchical organization of these systems generally plays a key role in their properties, function and survival (Fratzl and Weinkamer, 2007; Gibson et al., 2010). Hierarchy is also important in engineering designs, materials and architecture. Examples range from the Eiffel tower (Lakes, 1993) and polymers with micro-level hierarchical structures (Lakes, 1993), to sandwich panels with cores made of foams or composite lattice structures (Cote et al., 2009; Fan et al., 2008; Kazemahvazi et al., 2009; Kazemahvazi and Zenkert, 2009; Kooistra et al., 2007). There, the hierarchical organization can lead to superior mechanical behavior and tailorable properties, as described recently for sandwich cores with hierarchical structure (Fan et al., 2008) and for hierarchical corrugated truss structures (Kooistra et al., 2007). The overall mechanical behavior of these structures is governed by the response at different length scales and levels of hierarchy; and increasing levels of structural hierarchy can result in lighter-weight and better-performing structures (Bhat et al., 1989; Burgueño et al., 2005; Gibson et al., 2010; Kooistra et al., 2007; Lakes, 1993; Murphey and Hinkle, 2003; Taylor et al., 2011).

Here, we have presented a systematic way to incorporate hierarchy in honeycomb structures. Honeycombs are two-dimensional cellular structures used in different applications including thermal isolation (Lu and Chen, 1999), impact energy absorption and structural protection (Ajdari et al., 2011; Vaziri and Hutchinson, 2007; Zheng et al., 2005), and as the core of lightweight sandwich panels (Rathbun et al., 2006; Xue and Hutchinson, 2004; Xue and

Hutchinson, 2006). The transverse (i.e., in-plane) stiffness and strength of honeycombs are generally governed by the bending deformation of cell walls, and strongly depend on the honeycomb relative density (Gibson, 1997). Under uniform transverse loading, the maximum bending moment in each cell wall occurs at the honeycomb vertices (i.e., cell wall corners). Thus, moving material from the middle part of each wall closer to the vertices can potentially increase the transverse stiffness and strength (Chuang and Huang, 2002a, b; Simone and Gibson, 1998). Here, we replace the vertices of a regular hexagonal lattice with smaller hexagons (simultaneously reducing the wall thickness to maintain fixed overall density), to achieve a structure with one level of hierarchy. This will be shown able to exhibit a Young's modulus superior to that of its regular hexagonal counterpart of equal relative density. This replacement procedure for three-edge vertices can be repeated at smaller scales to achieve fractal-appearing honeycombs with higher orders of structural hierarchy. Figure 5-1-A shows the evolution of a hexagonal honeycomb cell as structural hierarchy is increased. The structural organization of the honeycomb at each level of hierarchy can be defined by the ratio of the introduced hexagonal edge length (b for 1st order hierarchy and c for 2nd order hierarchy), to the original hexagon's edge length, a, as described in Figure 5-1-A (i.e., $\gamma_1 = b/a$ and $\gamma_2 = c/a$). For a honeycomb with 1st order hierarchy, $0 \leq b \leq a/2$ and thus, $0 \leq \gamma_1 \leq 0.5$, where $\gamma_1 = 0$ denotes the regular honeycomb structure. For a honeycomb with 2nd order hierarchy, there are two geometrical constraints, $0 \leq c \leq b$ and $c \leq a/2-b$. In terms of the ratio parameters, the constraints are $0 \leq \gamma_2 \leq \gamma_1$ if $\gamma_1 \leq 0.25$ and $0 \leq \gamma_2 \leq (0.5 - \gamma_1)$ if $0.25 \leq \gamma_1 \leq 0.5$. The dimensionless relative density (i.e., area fraction), can be given in terms of t/a:

$$\rho = 2/\sqrt{3} \cdot (1 + 2\gamma_1 + 6\gamma_2) \cdot t/a, \quad (1)$$

where t is the thickness of the cell walls, from which the special cases of γ_2, γ_1 = 0 can be read off immediately. (For regular honeycomb, $\rho = 2/\sqrt{3} \cdot t/a$; and for honeycomb with 1st order hierarchy, $\rho = 2/\sqrt{3} \cdot (1 + 2\gamma_1) \cdot t/a$). This relation clearly shows that t/a must decrease to maintain fixed relative density as γ_1, γ_2 are increased.

Here, we studied the effective elastic properties hierarchical honeycombs using analytical, numerical and experimental methods. The hierarchical honeycomb samples were fabricated using 3D printing as discussed in section 5.2. In sections 5.3and 5.4, we provided analytical models to estimate the effective elastic modulus and Poisson's ratio of hierarchical honeycombs using the concepts of mechanics of materials and compare the analytical results with finite element simulations and experiments.

5.2 Fabrication using 3D printing

Figure 5-1-B shows samples of regular and hierarchical honeycombs with ρ = 0.10 and a = 20 mm fabricated using 3D printing (Dimensions 3D printer, Stratasys Inc., Eden Prairie, MN). The regular honeycomb has t = 1.75mm; the honeycomb with one-level hierarchy has γ_1= 0.3 and t = 1mm; and that with two-level hierarchy has γ_1= 0.3, γ_2= 0.12, and t = 0.75mm. These were printed as three-dimensional extruded shells from an ABS polymer (acrylonitrile butadiene styrene, elastic modulus = 2.3 GPa) as the bulk material. The input file to the 3D printing software was created for honeycombs with a relative density of 0.10. The cell wall thickness was reduced for honeycombs with hierarchy in order to keep the overall relative density constant, similar to the finite element calculations. The actual printed samples did not maintain the target density very precisely due to the 0.25 mm resolution of the printer (so the relative density was between 8-12%, and only certain discrete values of γ_1 and $\gamma_2$could be achieved). Prior to the experiments, aluminum plates were bonded to the top and bottom of the samples using

cyanoacrylate adhesive, in order to prevent the edge nodes (similar to 1, 2, 3, and 4 in Figure 5-2) from excessive bending. The in-plane compressive response of these bonded-end samples was measured using an INSTRON 5582 at the slow rate of 1mm/min (i.e., strain rate, $\dot{\varepsilon} = 0.5\%/\text{min}$). The effective elastic modulus of the honeycombs were estimated from the slope of the force-displacement curve at early stage of the experiment ($\varepsilon < 1.5\%$). For each specimen, the true relative density was measured by weighing, and then was used when calculating the normalized effective elastic modulus for Figure 5-3. For each configuration, three samples were tested. In addition to the experiments, we developed analytical and finite element models to calculate the effective in-plane elastic constants of the honeycombs in terms of cell-wall Young's modulus.

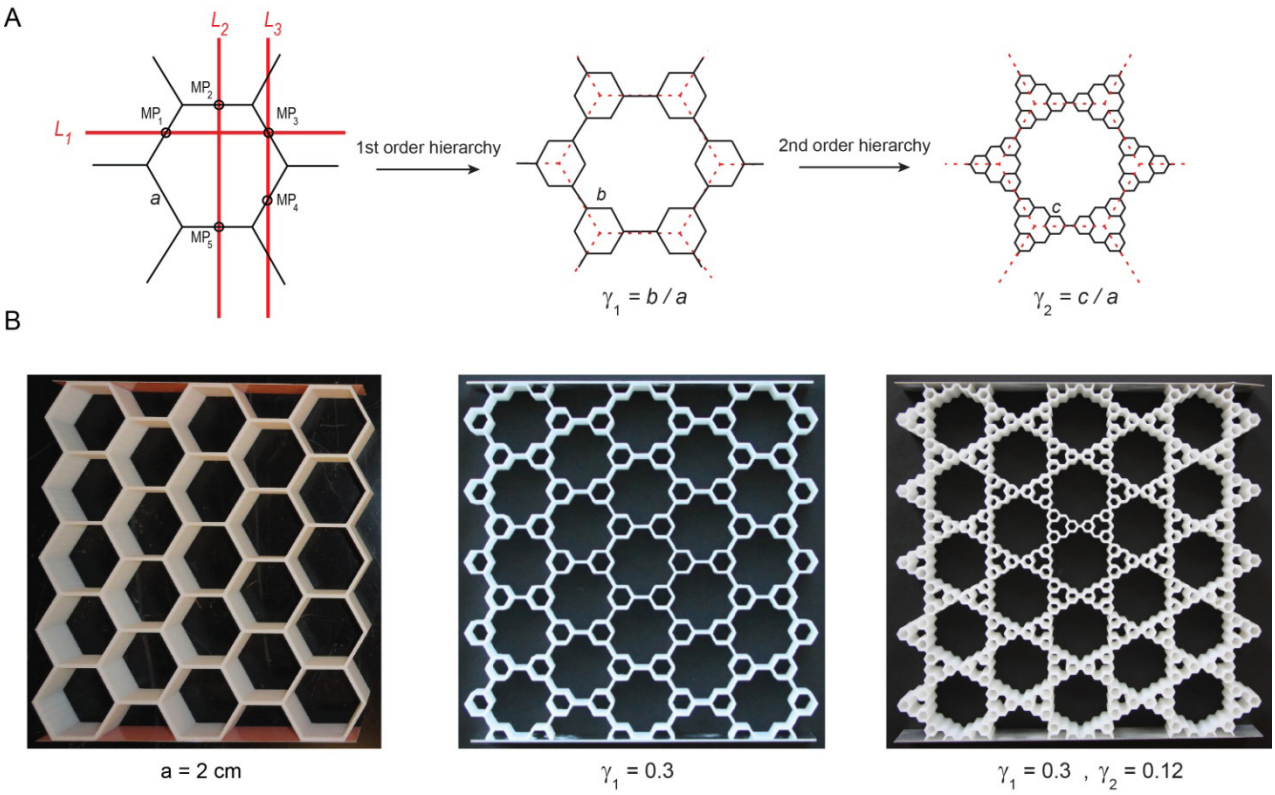

Figure 5-1- Hierarchical honeycombs. (A) Unit cell of the hierarchical honeycombs with regular structure and with 1st and 2nd order hierarchy. (B) Images of honeycombs with a = 2 cm fabricated using three-dimensional printing.

5.3 Hierarchical honeycombs: Effective elastic modulus - Analytical approach

For the analytical approach, we used Castigliano's second theorem (Boresi, 2002) to determine the uniaxial in-plane deformation of hierarchical honeycombs made of an isotropic elastic material with elastic modulus, E_s. It is well known that plane lattices with threefold symmetry will exhibit macroscopically isotropic in-plane elastic behavior (Christensen, 1987). Thus, the macroscopic in-plane linear elastic behavior of hierarchical honeycomb can be characterized by just two constants, to be found by whatever loadings are most convenient. We imposed a far field y-direction stress, $\sigma_{yy} = -(2/\sqrt{3})F/a$, in a vertical direction (perpendicular to the horizontal hexagon edges in Figure 5-1-A). This is equivalent to applying a vertical force F at every cut-point of a horizontal line (such as L_1 in Figure 5-1-A) passing through the mid-points of non-horizontal edges in a row of underlying (i.e., no hierarchy) hexagons.

To understand the analysis, it is helpful to envision the underlying regular hexagonal network as illustrated in Figure 5-1-A. Midpoints of various edges have been labeled MP_1 to MP_5. For the imposed state of stress, no net horizontal or vertical force is transmitted across L_2. Yet every horizontal bar is equivalent, allowing us to conclude that each one transmits neither axial nor shear force. Furthermore, they also transmit no bending moment, because it would break the symmetry about horizontal lines. Therefore, the horizontal edges are entirely load-free for this state of stress. Next, considering the edges cut at their midpoints by line L_1, it is clear that for the given average stress, each cut bar must sustain a vertical force F. Cut at the midpoints as they are, we can conclude that no moment is transmitted across the cut, because that would lead to the bars being bulged 'out' of some hexagons and 'into' others, in a way prohibited by the symmetry of reflecting in L_1. The stress state also implies that no net horizontal force is transmitted across L_1. Therefore, considering the structure below L_1, a leftward force at MP_3

balanced by a rightward force at MP_1 might be envisaged. But by reflection in a horizontal line through the hexagon center, we would also have to expect a leftward force on the bar *above* a cut at MP_4. The resulting net leftward force on the bars between cuts at MP_3 and MP_4 is not possible because we already know that the horizontal bars (e.g., on the line through the hexagon center) are tension-free. We can thus conclude that the forces at cut points MP_1, MP_3 , and MP_4 are purely vertical with magnitude F. This 'hexagon midpoint' reasoning is unchanged when structural hierarchy is introduced.

Figure 5-2-A shows the free body diagram of a subassembly able to represent an entire honeycomb with 1st order hierarchy subject to σ_{yy} loading (therefore, for this section, to find effective elastic modulus in y-direction, we are ignoring the horizontal forces shown at point 2,3, and 4). According to the above arguments, MP_3 is load-free, and MP_4 is subject only to force $-F$ in the y direction. Since the subassembly is also cut free at points 1 and 2, we need to find the force and moment reactions at those cuts. y-direction forces acting on the subassembly are denoted by N_1 and N_2, and moments are denoted by M_1 and M_2. There can be no horizontal force at point 1 because of reflection symmetry about the x axis, along with the lack of any third force on point 1 to balance same-direction horizontal inputs from above and below. At point 2, since no other horizontal forces act on the subassembly, we can also be sure that there is no horizontal reaction. So in this problem, x -direction equilibrium is trivially satisfied. By applying the y-force and moment balance laws to the subassembly, N_2 and M_2 can therefore be written as linear functions of N_1, M_1, and F. The bending energy stored in the subassembly can be expressed as a sum over all the beams: $U(F, M_1, N_1) = \sum \int (M^2/(2E_s I))ds$, where M is the bending moment at location s along the beam, E_s is the elastic modulus of the cell wall material, and I is the beam's cross sectional area moment of inertia at s (cell walls are considered to have rectangular cross

section with thickness, t , and unit depth; i.e., $I = t^3/12$). Since the beam resultants are linear in F, M_1 and N_1, U is then a quadratic function of those same quantities. The horizontal beam connecting nodes 2 and 3 can be excluded from the analysis since it is load-free.

Since there is zero vertical displacement and zero rotation at point 1 due to symmetry, we can use Castigliano's method to write $\partial U/\partial N_1 = 0$, and $\partial U/\partial M_1 = 0$. These two relations allow N_1 and M_1 to be calculated in terms of F: $N_1 = F(0.533 + 0.15/\gamma_1)$, $M_1 = Fa(0.283\gamma_1 - 0.017)$. At point 4 we can find the displacement $\delta = \partial U/\partial F$, and then the above substitution for N_1 and M_1 gives $\delta = \sqrt{3}Fa^3/\big(72EIf(\gamma_1)\big)$. The effective elastic modulus (to be normalized by beam material modulus, E_s) is then defined as the ratio of average stress ($-2F/3a$) and average strain, ($-4\delta/a\sqrt{3}$) :

$$E/E_s = (t/a)^3\, f(\gamma_1) \tag{2}$$

where $f(\gamma_1) = \sqrt{3}/(0.75 - 3.525\gamma_1 + 3.6\gamma_1^2 + 2.9\gamma_1^3)$. To find the maximum normalized elastic modulus for structures with first-level hierarchy and constant relative density, we eliminate *(t/a)* from Eq. (2) by using the relative density expression of Eq. (1) The resulting expression for E/E_s is ρ^3 times a function of γ_1, and setting $(\partial(E/E_s)/\partial\gamma_1)_\rho = 0$ gives γ_1= 0.32. Making this substitution leads to $E/E_s = 2.97\rho^3$, a stiffness almost twice the stiffness of the regular honeycomb structure(Gibson, 1997), for which $E_0/E_s = 1.5\rho^3$. (The regular honeycomb result can be found by letting $\gamma_1 = 0$ in Eq. (2), and using Eq. (1) to eliminate *t/a*).

The same analytical approach was used to evaluate the in-plane effective Young's modulus of honeycomb with two orders of hierarchy, as a function of hierarchy indices γ_1 and γ_2. Figure 5-2-B shows the free body diagram of a subassembly chosen to minimize calculation. As before, the vertical compressive stress (*-2F/3a*) is achieved by the external force, *F*, applied

downward at point 5 (a midpoint of the underlying hexagon side), with symmetry arguments showing that no other loads act at that point. Bar 3-4 is again load-free. The same argument applies to point 3 as formerly applied to point 2 for the honeycomb with one order of hierarchy. And, the same argument applies to points 2 and 1 as formerly applied to point 1. Therefore, N_1, M_1, N_2, M_2, N_3, and M_3 are the unknown reaction forces and moments at vertices 1, 2, and 3 as shown in Figure 5-2-B. One additional step required for analysis of the second-order hierarchy is to determine the beam resultants for the statically indeterminate, complete (small) hexagon of side c embedded in each subassembly, loaded at nodes 6 and 7 with reactions at node 8. The bending moments along each side of the c-hexagon are determined from a subsidiary analysis in which it is divided at nodes 6 and 7, and then three compatibility conditions are enforced at each of those nodes. The details of that analysis are omitted for brevity. Similar to honeycombs with first order hierarchy, using the *y*-direction and rotational equilibrium equations, N_3 and M_3 can be written as a function of N_1, M_1, N_2, M_2, and F. Therefore, the total energy of the investigated substructure, which is the sum of the bending strain energy of all the beams, can be written as: $U(F, M_1, N_1, M_2, N_2) = \sum \int (M^2/(2E_s I))ds$. The following four boundary conditions are imposed at points 1 and 2 to achieve the zero rotation and zero displacement demanded by symmetry, as shown in Figure 5-2-B: $\partial U/\partial N_1 = 0$, $\partial U/\partial M_1 = 0$, $\partial U/\partial N_2 = 0$, and $\partial U/\partial M_2 = 0$. These relations allow us to solve for M_1, N_1, M_2, N_2. In a similar way as above the effective elastic modulus can be presented as:

$$E/E_s = (t/a)^3 f(\gamma_1, \xi) \tag{3}$$

where $\xi = \gamma_2/\gamma_1$ and $f(\gamma_1, \xi) = N_4(\xi)/(\gamma_1^3 D_7(\xi) + \gamma_1^2 D_6(\xi) + \gamma_1 D_5(\xi) + D_4(\xi))$

$N_4(\xi) = 29.62 - 54.26\xi + 31.75\xi^2 - 4.73\xi^3 - \xi^4$

$D_7(\xi) = 49.64 - 609.01\xi + 862.56\xi^2 - 195.50\xi^3 - 270.14\xi^4 + 159.95\xi^5 - 18.13\xi^6 - 2.20\xi^7$

$D_6(\xi) = 61.73 + 310.43\xi - 662.32\xi^2 + 334.12\xi^3 + 9.70\xi^4 - 29.38\xi^5 - 1.88\xi^6$

$D_5(\xi) = 60.43 + 12.80\xi + 123.22\xi^2 - 108.06\xi^3 + 20.50\xi^4 + 3.90\xi^5$

$D_4(\xi) = 12.80 - 23.46\xi + 13.74\xi^2 + 2.04\xi^3 - 0.43\xi^4$

For the 2nd order hierarchical structure, once again eliminating (*t/a*) in favor of density, and then differentiating at constant density, $((\partial(E/E_s)/\partial\gamma_1)_\rho = (\partial(E/E_s)/\partial\gamma_2)_\rho = 0$ give γ_1= 0.32, and γ_2= 0.135, leading to $E/E_s = 5.26\rho^3$, a stiffness almost 3.5 times that of the regular honeycomb.

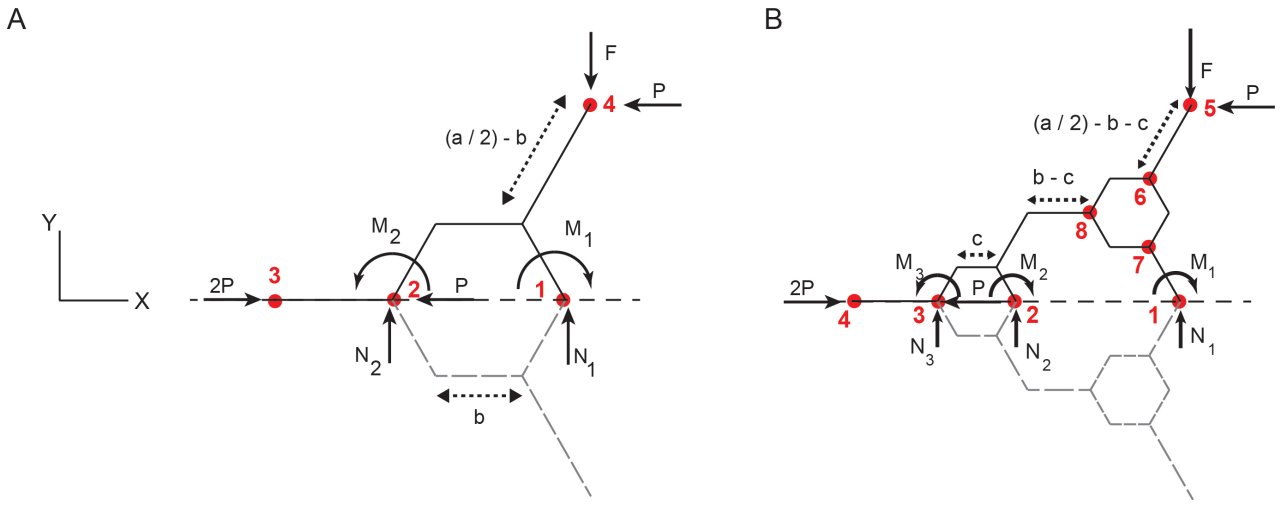

Figure 5-2- Free body diagrams of the subassembly of honeycombs with (A) 1st and (B) 2nd order hierarchy used in the analytical estimation. N_i and M_i (i= 1 to 3) denote the reaction vertical forces and moments in the nodes of the subassembly structures as denoted in the pictures.

5.4 Hierarchical honeycombs: Effective elastic modulus - Numerical simulation

To validate the theoretical results we simulated the structural response using finite element analysis. Two-dimensional hierarchical honeycombs were modeled using Abaqus 6.10 (SIMULIA, Providence, RI). All models were meshed using the BEAM22 element, which is capable of capturing not only the bending compliance of the above theory, but also the axial and shear deformations which may become significant at greater values of *t/a*. A rectangular cross section with unit length normal to the plane of loading was assumed for the cell wall beams. The thickness of all the beams was adjusted to control the overall relative density of the structure. The material properties of aluminum, E_s=70 GPa, and ν_s = 0.3, were used in this study. We performed the analysis with two different boundary conditions representing our analytical model and experimental tests, respectively. In the first set, we applied periodic boundary conditions to matching nodes on the left and right edges, as if the sample were infinitely wide but free to strain laterally (Harders et al., 2005). In the loading (vertical) direction, the structure was connected to a movable rigid plate by the nodes lying along the dashed symmetry line of Figure 5-2-A or Figure 5-2-B. Those nodes were constrained by symmetry conditions, i.e. free to slide left or right, but all maintaining the same y coordinate, and prevented from rotating. In the second set of simulations, those same top and bottom nodes were constrained horizontally by being built into the fixed and vertically movable rigid plates, and the side nodes were free as in the experimental setup. The increase in modulus caused by this constraint in the second kind of simulation ranged from 3% up to a maximum of about 20%. Here, we show the numerical results from the first set, which matched the boundary conditions of our analytical model. The effective elastic modulus of each structure was calculated from the slope of compressive stress-strain response.

Figure 5-3-A shows the effective elastic modulus of first order hierarchical honeycombs for all possible values of γ_1. In this figure, the elastic modulus is normalized by the effective stiffness of the counterpart regular honeycomb with the same relative density, $1.5E_s\rho^3$, allowing us to present results for every density on a single curve. In the finite element simulations, structures with three different relative densities (2%, 6% and 10%) were analyzed. Results show quite good agreement between numerical and theoretical approaches, even though the theoretical analysis ignored the axial and shear deformation of the beams (a good approximation only for low density honeycombs with small beam thickness (Harders et al., 2005)). We suspect that the numerical incorporation of shear and stretching accounts for the FEA-determined modulus falling somewhat below the theory, particularly as density increases or beam lengths decrease. The FEA results nicely confirm the near-doubling of stiffness for γ_1= 0.32. In this figure, experimental results are also plotted which show reasonable agreement with both theory and numerical results. For honeycombs with 2nd order hierarchy, we fixed γ_1= 0.3 and plotted the normalized effective elastic modulus for various values of γ_2, Figure 5-3-B. The results again match theory best for low density, and show that honeycombs with two orders of hierarchy where γ_1= 0.3, and γ_2= 0.135, have stiffness approximately 3.5 times that of regular hexagonal honeycomb with same relative density.

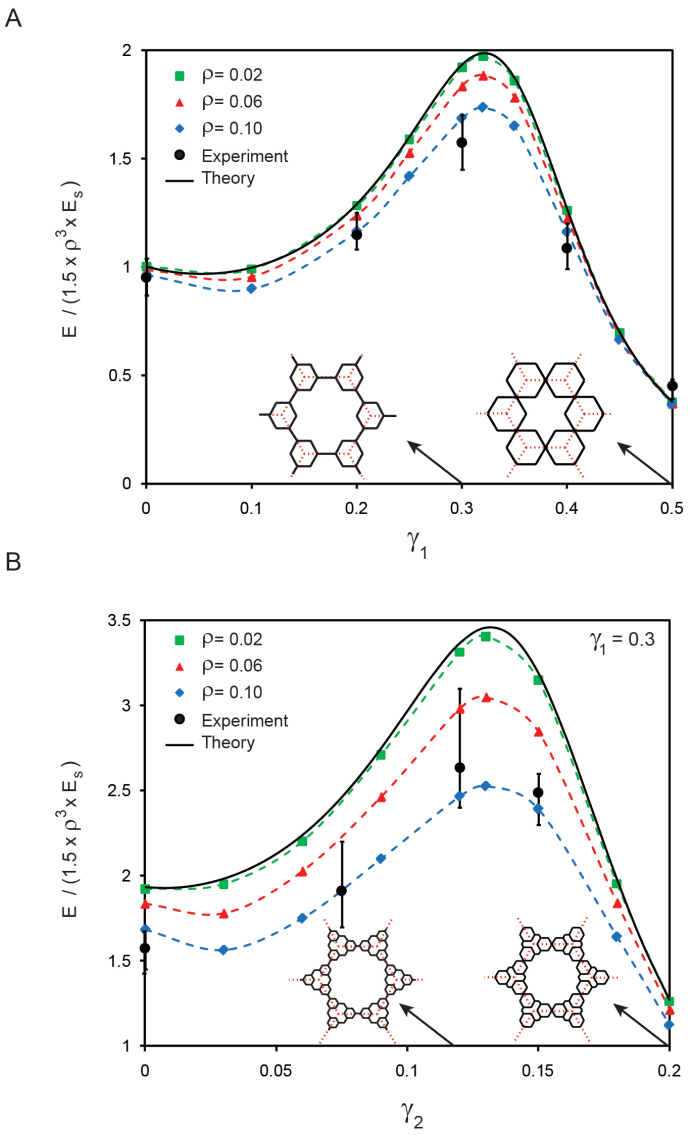

Figure 5-3- Stiffness of hierarchical honeycombs. (A) Normalized stiffness for honeycombs with 1st order hierarchy versus γ_1. (B) Normalized stiffness versus γ_2, for honeycombs with 2nd order hierarchy and γ_1= 0.3. The schematic of the honeycomb unit cells are shown for selected values of γ_1 and γ_2 in each plot. The finite element results are shown for honeycombs with three different relative densities. Experimental results for structures with different hierarchy levels are also shown (black circles). The error bars show the results variation. Each experimental point is from 3 tested specimens.

5.5 Hierarchical honeycombs: Poisson's ratio

To fully characterize the linear elastic behavior of hierarchical honeycombs, we also need to obtain the dependence of Poisson's ratio, ν, on the dimension ratios. We again used Castigliano's second theorem and considered the same subassemblies under biaxial loading (where the horizontal stress is finally set to zero after differentiating). This is a bending-based approximate analysis that ignores axial and shear deformation of the cell walls.

Temporarily considering horizontal loading only, we apply reasoning similar to that in section 5.4, to midpoint cut lines such as L_2 and L_3. This establishes that the horizontal segment aligned with the dotted line is subjected to pure compression (no bending), and that the segment midpoint to the upper right of each subassembly experiences only a horizontal force. There is no horizontal reaction at node 1 for first order hierarchy, or at nodes 1, 2 for second order hierarchy. But node 2 (first order) and node 3 (second order) has a horizontal reaction to balance 2P, -P, and nodes on the dashed horizontal line still require vertical and moment reactions. The composite free body diagrams for both horizontal and vertical stress are shown in Figure 5-2. Figure 5-2-A is for 1st order hierarchy where the external forces P and F are applied at point 4 in x- and y-directions, and N_1, M_1, N_2, and M_2 are the reaction vertical forces and moments at vertices 1 and 2, respectively. The two non-trivial equations of equilibrium (vertical and angular) allow us to write N_2 and M_2 as functions of N_1, M_1, P and F. Therefore, the bending energy stored in the subassembly can be expressed as the summation of bending energy in all beams, $U(F, P, M_1, N_1) = \sum \int (M^2/2E_sI)ds$, where M is the bending moment at position s along each beam, E_s is the elastic modulus of the cell wall material, and I is the beam's cross sectional area moment of inertia (cell walls are considered to have rectangular cross section with thickness t and unit depth, i.e., $I = t^3/12$). The horizontal beam connecting the nodes 2 and 3 can be

excluded from the analysis since it experiences no bending moment. Assuming zero displacement and zero rotation at vertices 1 and 2 due to symmetry, one can write $\partial U/\partial N_1 = 0$, and $\partial U/\partial M_1 = 0$. These two relations allow N_1 and M_1 to be calculated as a function of P and F. The bending energy stored in the subassembly can be subsequently expressed as $U = U(F, P)$. When P is zero (free lateral expansion), the x and y displacements of point 4 due to force F can be expressed as follows, respectively:$\delta_X^F = (\partial U/\partial P)|_{p=0}$; $\delta_Y^F = (\partial U/\partial F)|_{p=0}$. Considering the initial dimensions of the subassembly to be $3a/4$ and $\sqrt{3}a/4$ in X- and Y- dimensions, respectively, the Poisson's ratios in direction Y is obtained as $\nu = \delta_X^F/\sqrt{3}\delta_Y^F$, which gives: $\nu = 1 - {\gamma_1}^3/(2.9{\gamma_1}^3 + 3.6{\gamma_1}^2 - 3.525\gamma_1 + 0.75)$, which is plotted in Figure 5-4. The value of ν is $\nu = 1$ at $\gamma_1 = 0$, $\nu = 0.5$ at $\gamma_1 = 1$, with the minimum value 0.37 at $\gamma_1 = 0.4$. Finite element results are also shown which were obtained by calculating the lateral deformation of honeycombs with periodic boundary condition under uniaxial in-plane loading.

For the biaxially loaded 2nd order hierarchical honeycomb subassembly illustrated in Figure 5-2-B. N_1, M_1, N_2, M_2, N_3, and M_3 are the unknown reaction vertical forces and moments. Once again, vertical and rotational equilibrium equations allow us to write N_3 and M_3 as functions of N_1, M_1, N_2, M_2, P and F. Therefore, the bending energy stored in the subassembly can be expressed as the summation of bending energy in all beams, $U(F, P, M_1, N_1, M_2, N_2) = \sum \int (M^2/2E_sI)ds$. The horizontal beam connecting nodes 3 and 4 is again excluded from the analysis. Since symmetry prevents vertical displacement or rotation at vertices 1 and 2, one can write $\partial U/\partial N_1 = 0$, $\partial U/\partial M_1 = 0$, $\partial U/\partial N_2 = 0$, and $\partial U/\partial M_2 = 0$. These four relations allow N_1 , N_2 , M_1 and M_2 to be calculated as functions of P and F. The bending energy stored in the subassembly can be subsequently expressed as $U = U(F, P)$. The x and y displacements of point 5 due to force F can be expressed as: $\delta_X^F = (\partial U/\partial P)|_{p=0}$; $\delta_Y^F = (\partial U/\partial F)|_{p=0}$. Considering

the initial dimensions of the subassembly to be $3a/4$ and $\sqrt{3}a/4$in the *x* and *y* directions, the Poisson ratio is obtained as: $= \delta_X^F/\sqrt{3}\delta_Y^F$. The value of ν ranges from 0.28 at $\gamma_1 = \gamma_2 = 0.23$ to 1.0 at $\gamma_1 = \gamma_2 = 0$.

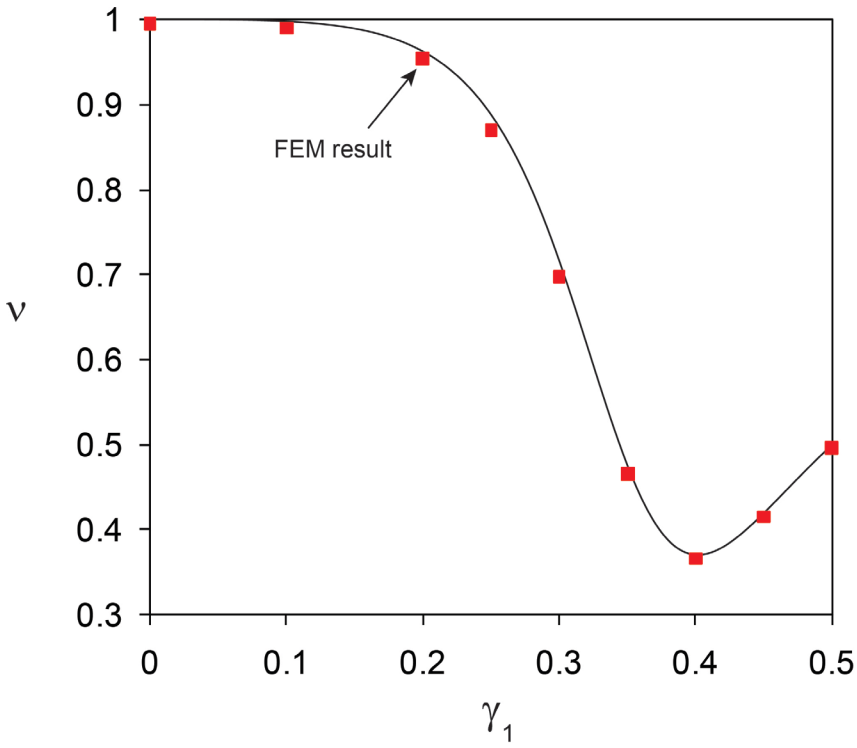

Figure 5-4- Poisson's ratio of hierarchical honeycombs with one level of hierarchy versus γ_1. The finite element results are also plotted for honeycomb with relative density 0.06.

6 CHAPTER 6: DYNAMIC CRUSHING OF HIERARCHICAL HONEYCOMBS

6.1 Background

As mentioned in previous chapters, one of the main applications of cellular structures is their usage in impact resistance and structural protection where their energy absorption characteristics become important. Besides, most biological system in nature has hierarchical organization. The hierarchical organization of these systems generally plays a key role in their properties, function and survival (Fratzl and Weinkamer, 2007; Gibson et al., 2010).

Hierarchy is also important in engineering designs, materials and architecture. Examples range from the Eiffel tower (Lakes, 1993) and polymers with micro-level hierarchical structures (Lakes, 1993), to sandwich panels with cores made of foams or composite lattice structures (Cote et al., 2009; Fan et al., 2008; Kazemahvazi et al., 2009; Kazemahvazi and Zenkert, 2009; Kooistra et al., 2007). There, the hierarchical organization can lead to superior mechanical behavior and tailorable properties, as described recently for sandwich cores with hierarchical structure (Fan et al., 2008) and for hierarchical corrugated truss structures (Kooistra et al., 2007). Enhancement up to one order of magnitude was reported for mechanical properties of honeycombs with 2nd order hierarchical sandwich walls by (Fan et al., 2008).

In this chapter, we will study the energy absorption of honeycombs with 1st order of hierarchy. As an addition to previous chapters, we have also considered the plastic hardening in the cell wall's material to show the enhancement of hierarchical honeycombs compare to regular hexagonal honeycombs.

6.2 Dynamic response of honeycombs with one order of hierarchy - Low crushing rate

Models of honeycombs with different ratio of hierarchical indices are simulated using ABAQUS (SIMULIA, Providence, RI). Same boundary conditions as described in Chapter 2

were used and plastic dissipation of honeycombs with same relative density under low velocity crushing was compared up to high crushing strain while changing the hierarchical index, γ_1. First, we considered the material of the cell walls to be linear elastic-perfectly plastic.

In Figure 6-1, we have plotted the normalized plastic dissipation for hierarchical honeycomb structures with $\gamma_1 = 0.3$ and $\gamma_1 = 0$ (regular honeycomb structure). At early stages of crushing, both structures show similar energy absorption capacity. An interesting behavior is observed for hierarchical structure, where at ~ 70% crushing strain, the normalized plastic dissipation increases significantly compare to regular honeycomb structure with the same relative density, as quantified in Figure 6-1.

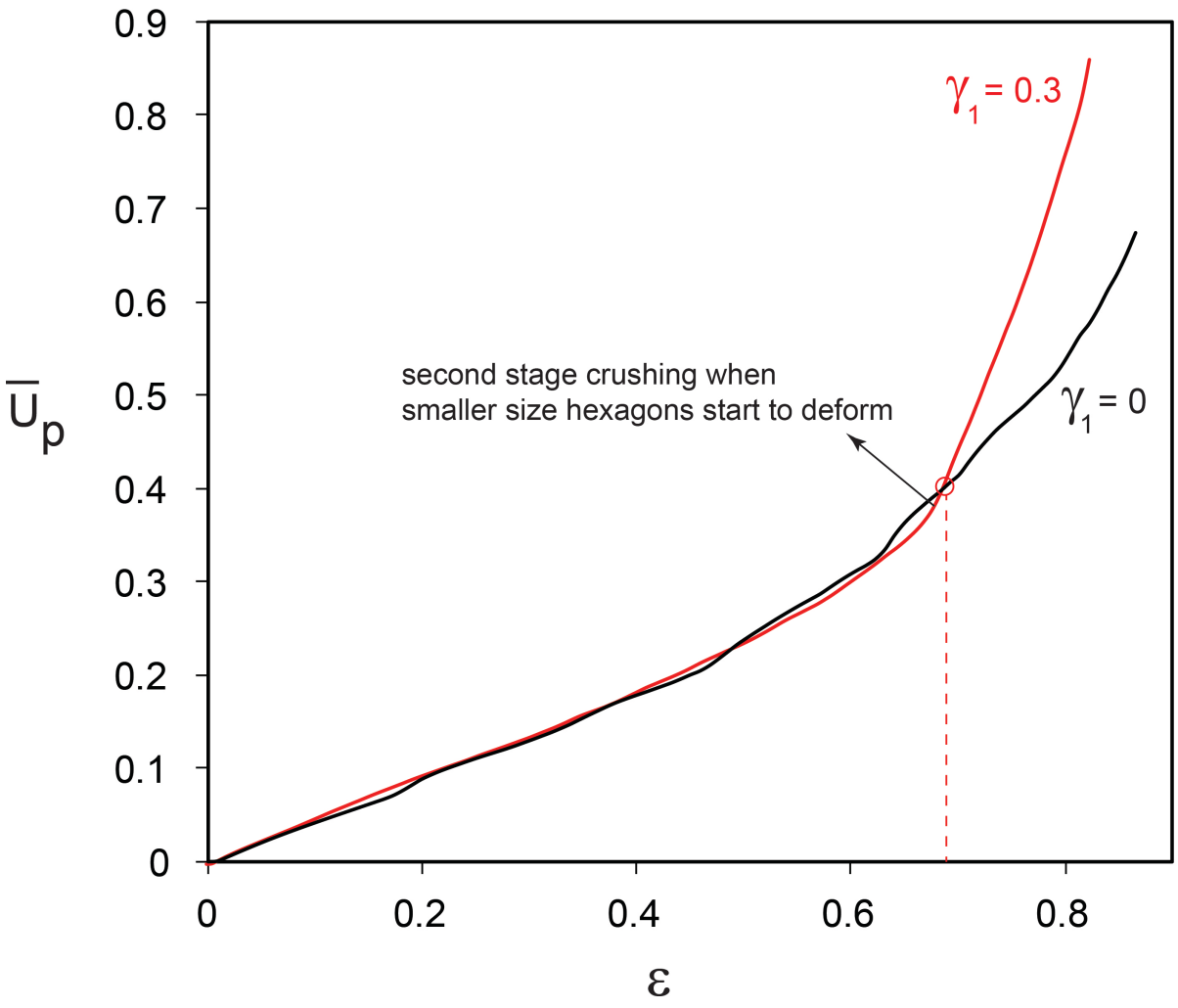

Figure 6-1 - Normalized plastic dissipation for hierarchical honeycomb at low crushing rate ($\bar{V} = 0.32$) with $\gamma_1 = 0$ and $\gamma_1 = 0.3$. The curve shows the significant increase in the plastic dissipation at crushing strain of ~70%.

To explain the reason we looked at the deformation pattern of the structures under low velocity crushing, as shown in Figure 6-2. In this figure, we have plotted the force-displacement response of both regular and hierarchical honeycomb with one order of hierarchy and $\gamma_1 = 0.3$. Black line shows the response for regular hexagonal honeycomb: typical elastic response at early stage of crushing which results in linear increase of the force/stress, followed by the plateau border where the force(stress level) is almost constant and final densification with significant increase of the stress. The red line shows the response for hierarchical honeycomb where $\gamma_1 = 0.3$. The response of honeycomb with two order of hierarchy is also shown (blue line).

As described in chapter 2, for regular honeycomb structure, under low crushing rate, with the boundary conditions explained before, we saw an *X-shape mode* where shear bands in the form of "X" is observed. For honeycombs with first order of hierarchy, at early stage of the crushing, all the cell walls belongs to the bigger hexagons starts to deform and form the exact *X-shape*, as shown in the Figure 6-2, this is the case up to almost 70% crushing. Further crushing will results in significant increase in the plastic dissipation and/or force, as illustrated in Figure 6-1 and Figure 6-2. At this stage of crushing, cell walls belongs to the smaller size hexagons come to the picture and start to deform, which will increase the number of plastic hinges and will results in higher energy absorption. The crushing strain at which the second stage of crushing happens, depends on the geometrical parameter γ_1, for example for $\gamma_1 = 0.45$, the second stage of crushing happens at ~55% crushing.

The response for honeycombs with two order of hierarchy, does not clearly show the multi-stage behavior when we have a uniform thickness all over the structures. However, we have confirmed that by distributing the mass properly between the hexagons at different level of hierarchy, the structure does show multi-stage behavior.

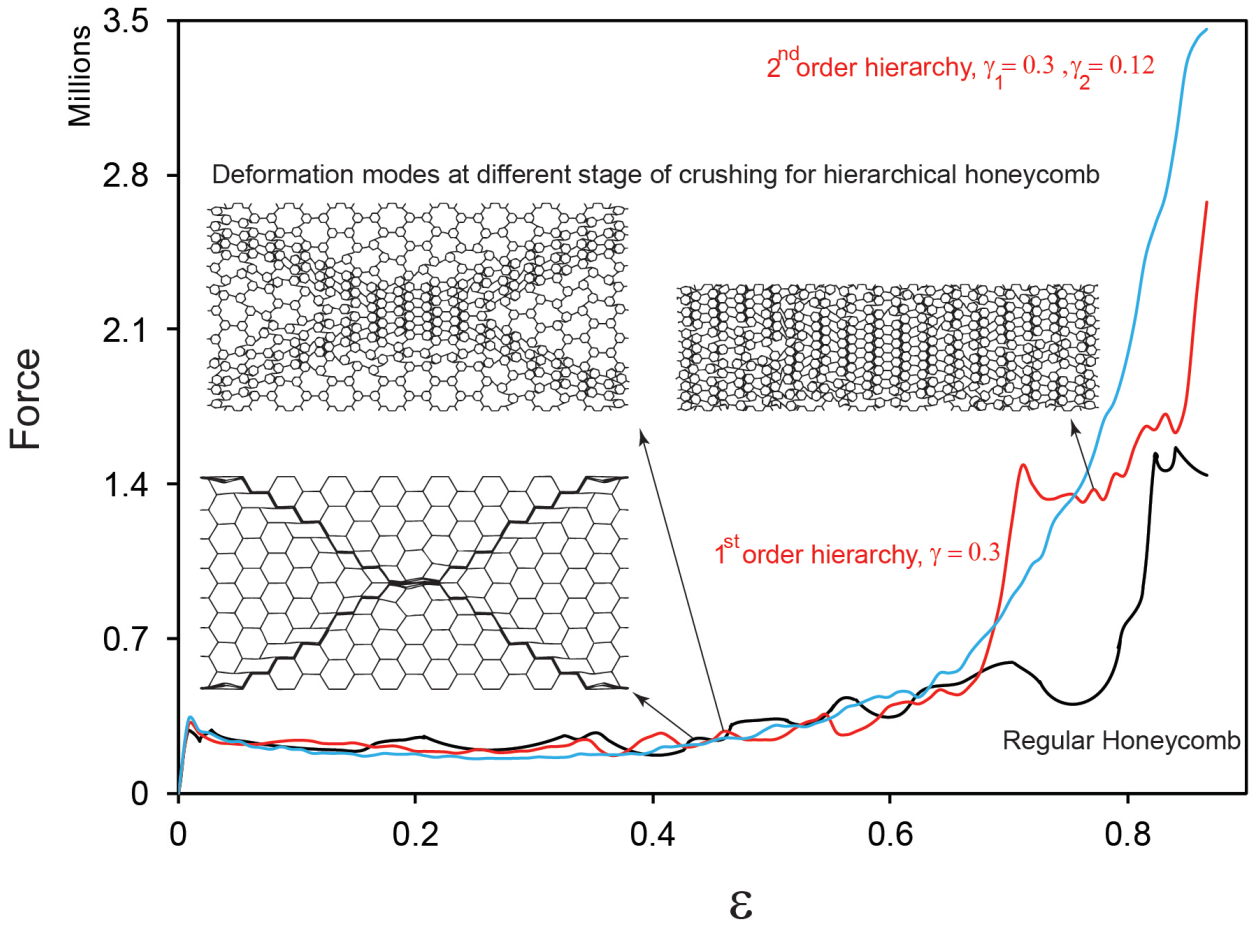

Figure 6-2 - Force-displacement response for hierarchical honeycomb under low crushing rate ($\bar{V} = 0.32$). Results for both regular and hierarchical honeycomb are shown. The multi-stage crushing of the hierarchical honeycomb is obvious.

6.3 Honeycombs with plastic hardening

When one level of hierarchy, as proposed in chapter 5, is introduced to a regular hexagonal honeycomb, by replacing the vertices of a regular hexagonal lattice with smaller hexagons, in fact we are increasing the total number of the plastic hinges in the entire structure, and therefore increasing the energy absorption of the structure. In previous chapters, for energy absorption and impact behavior of honeycombs, we assumed the cell wall material to be an elastic-perfectly plastic material. If the cell wall material has plastic hardening behavior, then the hierarchical honeycomb potentially will show better performance compare to regular honeycomb of the same mass. And for obvious reason, adding level of hierarchy, will add more plastic hinges and for materials with plastic hardening will results in significant plastic dissipation compare to regular, and hierarchical honeycomb with one level of hierarchy.

In Figure 6-3, we have summarized the normalized plastic dissipation for honeycombs with and without plastic hardening. Here, we have plotted the normalized plastic dissipation for honeycombs with $\gamma_1 = 0.1$ and regular hexagonal honeycomb ($\gamma_1 = 0$) for comparison. When there is no plastic hardening, the plastic dissipation increases by adding hierarchy (almost 50% increase at 50% crushing strain). By adding only 5% plastic hardening to the material of the cell walls, we increase the total plastic dissipation of the regular and hierarchical honeycomb, however, this increase is much more significant for hierarchical honeycombs due to larger number of plastic hinges in the structures which increases the yielding points and therefore results in more energy dissipation, as shown in Figure 6-3.

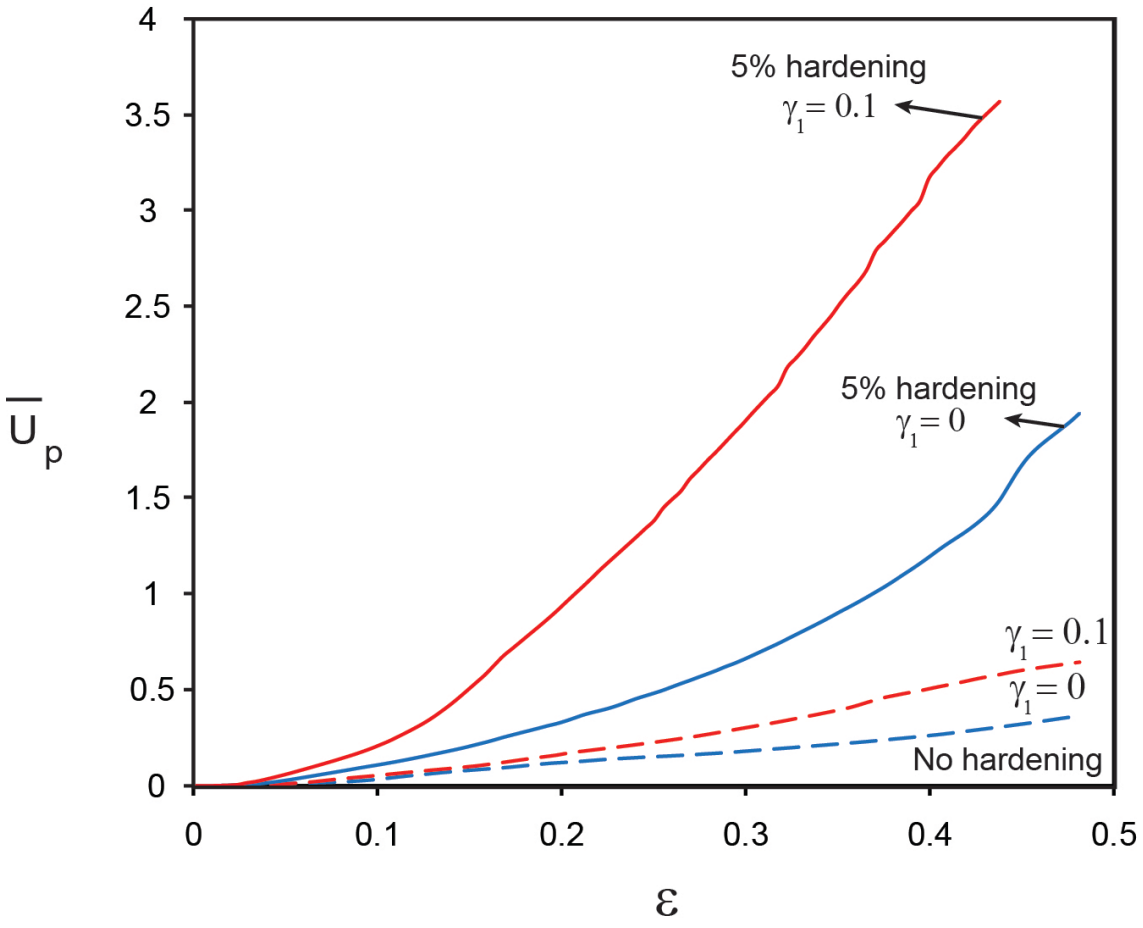

Figure 6-3 - Effect of plastic hardening on energy absorption of hierarchical honeycombs.

The multi-stage behavior of hierarchical honeycombs, which was observed in quasi-static crushing of these structures can be used as a tool to regulate the energy absorption under low crushing rates. By nature, adding the hierarchy to the structure, should results in higher energy absorption capacity, due to the increase in number of plastic hinges in the entire structure. by distributing the mass at different levels of hierarchy, we should be able to tailor the mechanical behavior as well as energy absorption capacitance of hierarchical honeycombs.

7 CHAPTER 7: CONCLUDING REMARKS

7.1 Summary

Finite element method was employed to study the in-plane crushing of regular, irregular and functionally graded honeycombs. Insights into the role of 'dynamics effects' on the overall energy absorption and impact resistant of cellular structures are provided, and different deformation modes for honeycombs subjected to dynamic crushing were identified. The role of irregularities, in the form of missing cell clusters and variations in the cell arrangements was also studied for a wide range of crushing velocities. Our results complement previous studies on the dynamic behavior of cellular structures with uniform cell size and wall thickness, while providing new insight into the role of deformation rate, defects and irregularity on the behavior of cellular structures under dynamic loading.

We also studied the dynamic crushing of functionally graded cellular structure with regular and irregular cellular arrangements. Our results show that introducing a density gradient could significantly change the deformation mode and energy absorption of cellular structures under both low and high crushing velocities. A limited number of functionally graded cellular structures were analyzed and no effort was made to obtain the cellular structure with maximum energy absorption at a constant average density. However, enough insight is provided to understand the mechanism of energy absorption in functionally graded cellular structures under dynamic loading. Our results could help better understand the behavior and function of some of the engineered and biological cellular materials. Our study also complements recent studies on performance of sandwich panels with graded cores (Dharmasena et al., 2009; Wang et al., 2009) and could help develop a new class of energy absorbent cellular materials and blast resistant structures.

To summarize the behavior of all honeycombs with the investigated hierarchical structures, we have plotted contour maps of the effective (normalized) elastic modulus and Poisson's ratio of hierarchical honeycombs with second-order hierarchy for all possible values of γ_1 and γ_2, as shown in Figure 7-1. The x-axis is γ_1 ranges from 0 to 0.5, while γ_2 is limited by the two geometrical constraints, $\gamma_2 \leq \gamma_1$ and $0 \leq \gamma_2 \leq (0.5 - \gamma_1)$. Hierarchical honeycombs with small to moderate values of γ_1 and γ_2, and especially a simple hexagonal honeycomb, have Poisson ratio near 1.0. This means that the Young's and Shear moduli, which are controlled by element bending, are far lower than the "Bulk" (really, "Areal") modulus which for those structures is controlled by element stretching.

The results show that a relatively broad range of elastic properties, and thus behavior, can be achieved by tailoring the structural organization of hierarchical honeycombs, and more specifically the two dimension ratios. Increasing the level of hierarchy provides a wider range of achievable properties. Further optimization should be possible by also varying the thickness of the hierarchically introduced cell walls, and thus the relative distribution of the mass, between different hierarchy levels. These hierarchical honeycombs can be used in development of novel lightweight multifunctional structures, for example as the cores of sandwich panels.

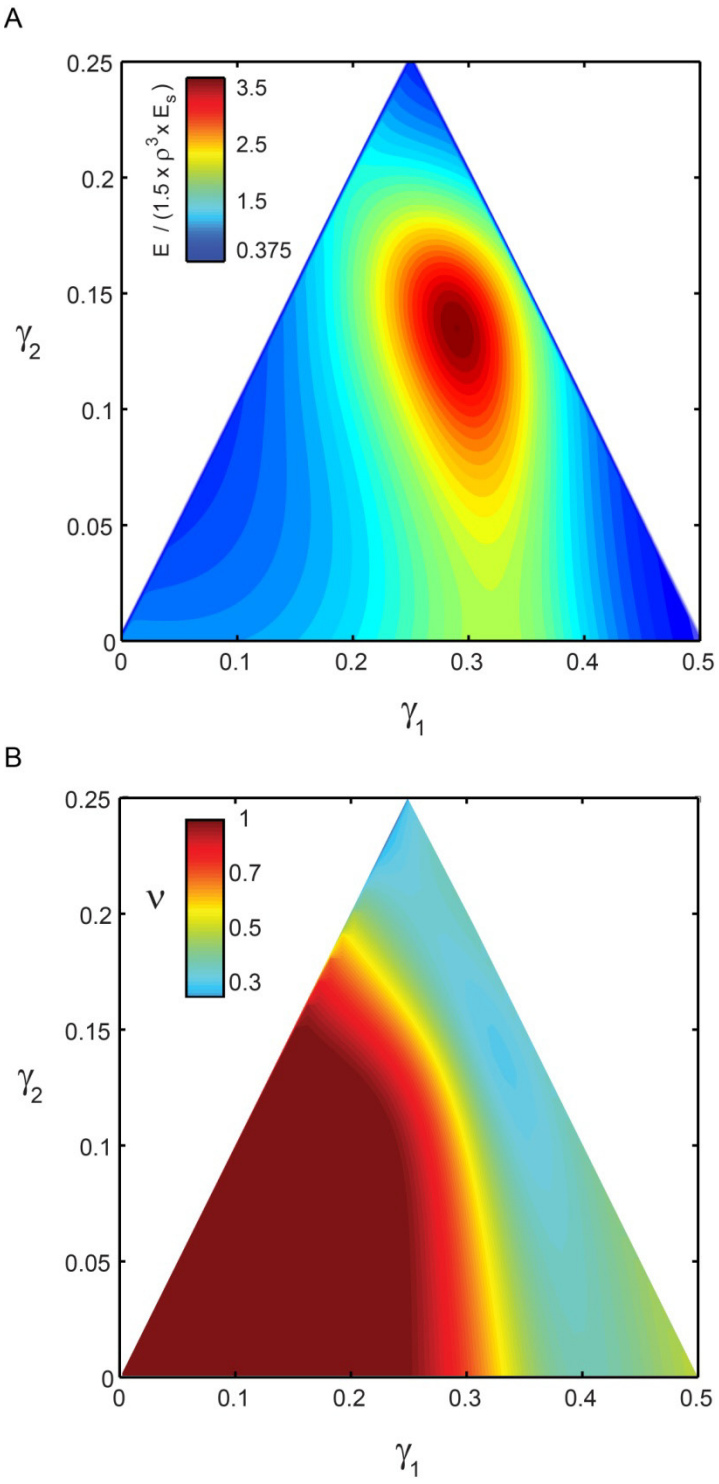

Figure 7-1- Contour maps of the (A) effective elastic modulus and (B) Poisson's ratio of hierarchical honeycombs with 2nd order hierarchy for all possible geometries (i.e., admissible range of γ_1 and γ_2).

8 CHAPTER 8: REFERENCES

- Abd El-Sayed, F.K., Jones, R., Burgess, I.W., 1979. A theoretical approach to the deformation of honeycomb based composite materials. Composites 10, 209-214.
- Aizenberg, J., Weaver, J.C., Thanawala, M.S., Sundar, V.C., Morse, D.E., Fratzl, P., 2005. Skeleton of Euplectella sp.: Structural Hierarchy from the Nanoscale to the Macroscale. Science 309, 275-278.
- Ajdari, A., Nayeb-Hashemi, H., Canavan, P., Warner, G., 2008. Effect of defects on elastic-plastic behavior of cellular materials. Materials Science and Engineering: A 487, 558-567.
- Ajdari, A., Nayeb-Hashemi, H., Vaziri, A., 2011. Dynamic crushing and energy absorption of regular, irregular and functionally graded cellular structures. International Journal of Solids and Structures 48, 506-516.
- Ali, M., Qamhiyah, A., Flugrad, D., Shakoor, M., 2008. Theoretical and finite element study of a compact energy absorber. Advances in Engineering Software 39, 95-106.
- Bhat, T., Wang, T.G., Gibson, L.J., 1989. Micro-sandwich honeycomb. SAMPE 25, 43-45.
- Boresi, A.P., Schmidt, R. J., 2002. Advanced Mechanics of Materials. Wiley.
- Buehler, M.J., 2006. Nature designs tough collagen: Explaining the nanostructure of collagen fibrils. Proceedings of the National Academy of Sciences 103, 12285-12290.
- Burgueño, R., Quagliata, M.J., Mohanty, A.K., Mehta, G., Drzal, L.T., Misra, M., 2005. Hierarchical cellular designs for load-bearing biocomposite beams and plates. Materials Science and Engineering A 390, 178-187.
- Chen, C., Lu, T.J., Fleck, N.A., 1999. Effect of imperfections on the yielding of two-dimensional foams. Journal of the Mechanics and Physics of Solids 47, 2235-2272.

- Chen, P.Y., Lin, A.Y.M., Lin, Y.S., Seki, Y., Stokes, A.G., Peyras, J., Olevsky, E.A., Meyers, M.A., McKittrick, J., 2008. Structure and mechanical properties of selected biological materials. Journal of the Mechanical Behavior of Biomedical Materials 1, 208-226.
- Christensen, R.M., 1987. Sufficient Symmetry Conditions for Isotropy of the Elastic Moduli Tensor. Journal of Applied Mechanics 54, 772-777.
- Chuang, C.-H., Huang, J.-S., 2002a. Effects of solid distribution on the elastic buckling of honeycombs. International Journal of Mechanical Sciences 44, 1429-1443.
- Chuang, C.-H., Huang, J.-S., 2002b. Elastic moduli and plastic collapse strength of hexagonal honeycombs with plateau borders. International Journal of Mechanical Sciences 44, 1827-1844.
- Cote, F., Russell, B.P., Deshpande, V.S., Fleck, N.A., 2009. The Through-Thickness Compressive Strength of a Composite Sandwich Panel With a Hierarchical Square Honeycomb Sandwich Core. Journal of Applied Mechanics 76, 061004-061008.
- Cui, L., Kiernan, S., Gilchrist, M.D., 2009. Designing the energy absorption capacity of functionally graded foam materials. Materials Science and Engineering: A 507, 215-225.
- Dharmasena, K., Queheillalt, D., Wadley, H., Chen, Y., Dudt, P., Knight, D., Wei, Z., Evans, A., 2009. Dynamic response of a multilayer prismatic structure to impulsive loads incident from water. International Journal of Impact Engineering 36, 632-643.
- Espinosa, H.D., Juster, A.L., Latourte, F.J., Loh, O.Y., Gregoire, D., Zavattieri, P.D., 2011. Tablet-level origin of toughening in abalone shells and translation to synthetic composite materials. Nat Commun 2, 173.
- Evans, A.G., Hutchinson, J.W., Ashby, M.F., 1998. Multifunctionality of cellular metal systems. Progress in Materials Science 43, 171-221.

- Fan, H.L., Jin, F.N., Fang, D.N., 2008. Mechanical properties of hierarchical cellular materials. Part I: Analysis. Composites Science and Technology 68, 3380-3387.
- Fazekas, A., Dendievel, R., Salvo, L., Bréchet, Y., 2002. Effect of microstructural topology upon the stiffness and strength of 2D cellular structures. International Journal of Mechanical Sciences 44, 2047-2066.
- Fleck, N.A., Deshpande, V.S., 2004. The Resistance of Clamped Sandwich Beams to Shock Loading. Journal of Applied Mechanics 71, 386-401.
- Fortes, M.A., Ashby, M.F., 1999. The effect of non-uniformity on the in-plane modulus of honeycombs. Acta Materialia 47, 3469-3473.
- Fratzl, P., Weinkamer, R., 2007. Nature's hierarchical materials. Progress in Materials Science 52, 1263-1334.
- Gent, A., 1963. Mechanics of Foamed Elastic Materials. Rubber Chem. Technol. 36, 597.
- Gent, A.N., Thomas, A.G., 1959. The deformation of foamed elastic materials. Journal of Applied Polymer Science 1, 107-113.
- Gibson, L.J., Ashby, M.F., Harley, B.A., 2010. Cellular materials in nature and medicine. Cambridge University Press.
- Gibson, L.J., Ashby, M.F., 1997. Cellular Solids: Structures and Properties, 2nd ed. Cambridge University Press, Cambridge.
- Guo, X.E., Gibson, L.J., 1999. Behavior of intact and damaged honeycombs: a finite element study. International Journal of Mechanical Sciences 41, 85-105.
- Harders, H., Hupfer, K., Rösler, J., 2005. Influence of cell wall shape and density on the mechanical behaviour of 2D foam structures. Acta Materialia 53, 1335-1345.
- Hollister, S.J., 2005. Porous scaffold design for tissue engineering. Nat Mater 4, 518-524.

- Hönig, A., Stronge, W.J., 2002a. In-plane dynamic crushing of honeycomb. Part I: crush band initiation and wave trapping. International Journal of Mechanical Sciences 44, 1665-1696.
- Hönig, A., Stronge, W.J., 2002b. In-plane dynamic crushing of honeycomb. Part II: application to impact. International Journal of Mechanical Sciences 44, 1697-1714.
- Hutchinson, J.W., Xue, Z., 2005. Metal sandwich plates optimized for pressure impulses. International Journal of Mechanical Sciences 47, 545-569.
- Hutmacher, D.W., 2000. Scaffolds in tissue engineering bone and cartilage. Biomaterials 21, 2529-2543.
- Jang, W.-Y., Kyriakides, S., 2009a. On the crushing of aluminum open-cell foams: Part I. Experiments. International Journal of Solids and Structures 46, 617-634.
- Jang, W.-Y., Kyriakides, S., 2009b. On the crushing of aluminum open-cell foams: Part II analysis. International Journal of Solids and Structures 46, 635-650.
- Kazemahvazi, S., Tanner, D., Zenkert, D., 2009. Corrugated all-composite sandwich structures. Part 2: Failure mechanisms and experimental programme. Composites Science and Technology 69, 920-925.
- Kazemahvazi, S., Zenkert, D., 2009. Corrugated all-composite sandwich structures. Part 1: Modeling. Composites Science and Technology 69, 913-919.
- Kiernan, S., Cui, L., Gilchrist, M.D., 2009. Propagation of a stress wave through a virtual functionally graded foam. International Journal of Non-Linear Mechanics 44, 456-468.
- Ko, W.L., 1965. Deformations of Foamed Elastomers. Journal of Cellular Plastics 1, 45-50.
- Kooistra, G.W., Deshpande, V., Wadley, H.N.G., 2007. Hierarchical Corrugated Core Sandwich Panel Concepts. Journal of Applied Mechanics 74, 259-268.
- Lakes, R., 1993. Materials with structural hierarchy. Nature 361, 511-515.

- Lederman, J.M., 1971. The prediction of the tensile properties of flexible foams. Journal of Applied Polymer Science 15, 693-703.
- Li, K., Gao, X.L., Wang, J., 2007. Dynamic crushing behavior of honeycomb structures with irregular cell shapes and non-uniform cell wall thickness. International Journal of Solids and Structures 44, 5003-5026.
- Liang, Y., Spuskanyuk, A.V., Flores, S.E., Hayhurst, D.R., Hutchinson, J.W., McMeeking, R.M., Evans, A.G., 2007. The Response of Metallic Sandwich Panels to Water Blast. Journal of Applied Mechanics 74, 81-99.
- Liu, Y., Zhang, X.-C., 2009. The influence of cell micro-topology on the in-plane dynamic crushing of honeycombs. International Journal of Impact Engineering 36, 98-109.
- Lu, T.J., Chen, C., 1999. Thermal transport and fire retardance properties of cellular aluminium alloys. Acta Materialia 47, 1469-1485.
- Menges, G., Knipschild, F., 1975. Estimation of mechanical properties for rigid polyurethane foams. Polymer Engineering & Science 15, 623-627.
- Mohr, D., Xue, Z., Vaziri, A., 2006. Quasi-static punch indentation of a honeycomb sandwich plate: experiments and constitutive modeling. Journal of Mechanics of Materials and Structures 1, 581-604.
- Mori, L., Queheillalt, D., Wadley, H., Espinosa, H., 2009. Deformation and Failure Modes of I-Core Sandwich Structures Subjected to Underwater Impulsive Loads. Experimental Mechanics 49, 257-275.
- Mori, L.F., Lee, S., Xue, Z.Y., Vaziri, A., Queheillalt, D.T., Dharmasena, K.P., Wadley, H.N.G., Hutchinson, J.W., Espinosa, H.D., 2007. Deformation and fracture modes of

sandwich structures subjected to underwater impulsive loads. Journal of Mechanics of Materials and Structures 2, 1981-2006.

- Murphey, T., Hinkle, J., 2003. Some performance trends in hierarchical truss structures, AIAA, Norfolk, VA, p. 1903.
- Nonell, J.B., Levick, M., 2001. Antonio Gaudi: Master Architect (Tiny Folio). Abbeville Press, New York, NY.
- Ortiz, C., Boyce, M.C., 2008. Bioinspired Structural Materials. Science 319, 1053-1054.
- Papka, S.D., Kyriakides, S., 1998. Experiments and full-scale numerical simulations of in-plane crushing of a honeycomb. Acta Materialia 46, 2765-2776.
- Qing, H., Mishnaevsky Jr, L., 2009. 3D hierarchical computational model of wood as a cellular material with fibril reinforced, heterogeneous multiple layers. Mechanics of Materials 41, 1034-1049.
- Rathbun, H.J., Radford, D.D., Xue, Z., He, M.Y., Yang, J., Deshpande, V., Fleck, N.A., Hutchinson, J.W., Zok, F.W., Evans, A.G., 2006. Performance of metallic honeycomb-core sandwich beams under shock loading. International Journal of Solids and Structures 43, 1746-1763.
- Ruan, D., Lu, G., Wang, B., Yu, T.X., 2003. In-plane dynamic crushing of honeycombs--a finite element study. International Journal of Impact Engineering 28, 161-182.
- Silva, E., Walters, M., Paulino, G., 2006. Modeling bamboo as a functionally graded material: lessons for the analysis of affordable materials. Journal of Materials Science 41, 6991-7004.
- Silva, M.J., Gibson, L.J., 1997. The effects of non-periodic microstructure and defects on the compressive strength of two-dimensional cellular solids. International Journal of Mechanical Sciences 39, 549-563.

- Silva, M.J., Hayes, W.C., Gibson, L.J., 1995. The effects of non-periodic microstructure on the elastic properties of two-dimensional cellular solids. International Journal of Mechanical Sciences 37, 1161-1177.
- Simone, A.E., Gibson, L.J., 1998. Effects of solid distribution on the stiffness and strength of metallic foams. Acta Materialia 46, 2139-2150.
- Tan, P.J., Reid, S.R., Harrigan, J.J., Zou, Z., Li, S., 2005. Dynamic compressive strength properties of aluminium foams. Part II--[`]shock' theory and comparison with experimental data and numerical models. Journal of the Mechanics and Physics of Solids 53, 2206-2230.
- Taylor, C.M., Smith, C.W., Miller, W., Evans, K.E., 2011. The effects of hierarchy on the in-plane elastic properties of honeycombs. International Journal of Solids and Structures 48, 1330-1339.
- Triantafyllidis, N., Schraad, M.W., 1998. Onset of failure in aluminum honeycombs under general in-plane loading. Journal of the Mechanics and Physics of Solids 46, 1089-1124.
- Vaughn, D.G., Hutchinson, J.W., 2005. Bucklewaves. European Journal of Mechanics - A/Solids 25, 1-12.
- Vaziri, A., Hutchinson, J.W., 2007. Metal sandwich plates subject to intense air shocks. International Journal of Solids and Structures 44, 2021-2035.
- Vaziri, A., Xue, Z., 2007. Mechanical behavior and constitutive modeling of metal cores. Journal of Mechanics of Materials and Structures 2, 1743-1760.
- Vaziri, A., Xue, Z., Hutchinson, J.W., 2007. Performance and failure of metal sandwich plates subjected to shock loading. J. Mechanics of Materials and Structures 2(10), 1947–1964.

- Wadley, H., Dharmasena, K., Chen, Y., Dudt, P., Knight, D., Charette, R., Kiddy, K., 2008. Compressive response of multilayered pyramidal lattices during underwater shock loading. International Journal of Impact Engineering 35, 1102-1114.
- Wadley, H.N.G., Dharmasena, K.P., Queheillalt, D.T., Chen, Y.C., Dudt, P., Knight, D., Kiddy, K., Xue, Z.Y., Vaziri, A., 2007. Dynamic compression of square honeycomb structures during underwater impulsive loading. Journal of Mechanics of Materials and Structures 2, 2025-2048.
- Wang, A.-J., McDowell, D.L., 2003. Effects of defects on in-plane properties of periodic metal honeycombs. International Journal of Mechanical Sciences 45, 1799-1813.
- Wang, E., Gardner, N., Shukla, A., 2009. The blast resistance of sandwich composites with stepwise graded cores. International Journal of Solids and Structures 46, 3492-3502.
- Wei, Z., Deshpande, V.S., Evans, A.G., Dharmasena, K.P., Queheillalt, D.T., Wadley, H.N.G., Murty, Y.V., Elzey, R.K., Dudt, P., Chen, Y., Knight, D., Kiddy, K., 2008. The resistance of metallic plates to localized impulse. Journal of the Mechanics and Physics of Solids 56, 2074-2091.
- Xue, Z., Hutchinson, J.W., 2003. Preliminary assessment of sandwich plates subject to blast loads. International Journal of Mechanical Sciences 45, 687-705.
- Xue, Z., Hutchinson, J.W., 2004. A comparative study of impulse-resistant metal sandwich plates. International Journal of Impact Engineering 30, 1283-1305.
- Xue, Z., Hutchinson, J.W., 2006. Crush dynamics of square honeycomb sandwich cores. International Journal for Numerical Methods in Engineering 65, 2221-2245.
- Zhao, H., Gary, G., 1998. CRUSHING BEHAVIOUR OF ALUMINIUM HONEYCOMBS UNDER IMPACT LOADING. International Journal of Impact Engineering 21, 827-836.

- Zheng, Z., Yu, J., Li, J., 2005. Dynamic crushing of 2D cellular structures: A finite element study. International Journal of Impact Engineering 32, 650-664.
- Zhu, H.X., Hobdell, J.R., Windle, A.H., 2001a. Effects of cell irregularity on the elastic properties of 2D Voronoi honeycombs. Journal of the Mechanics and Physics of Solids 49, 857-870.
- Zhu, H.X., Thorpe, S.M., Windle, A.H., 2001b. The geometrical properties of irregular two-dimensional Voronoi tessellations. Philosophical Magazine A 81, 2765 - 2783.
- Zou, Z., Reid, S.R., Tan, P.J., Li, S., Harrigan, J.J., 2009. Dynamic crushing of honeycombs and features of shock fronts. International Journal of Impact Engineering 36, 165-176.